MACHINABILITY INVESTIGATION OF RECYCLED SHORT CARBON FIBER REINFORCED MAGNESIUM MATRIX COMPOSITES

A Thesis Submitted to
the Graduate School of
İzmir Institute of Technology
in Partial Fulfillment of the Requirements for the Degree of

MASTER OF SCIENCE

in Mechanical Engineering

by
Şahin ATASOY

JULY 2023
İZMİR

We approve the thesis of **Şahin ATASOY**

Examining Committee Members:

Assoc. Prof. Dr. Sinan KANDEMİR
Department of Mechanical Engineering,
İzmir Institute of Technology

Assist. Prof. Dr. M. Fatih TOKSOY
Department of Mechanical Engineering,
İzmir Institute of Technology

Assoc. Prof. Dr. Levent AYDIN
Department of Mechanical Engineering,
İzmir Katip Çelebi University

07/July/2023

Assoc. Prof. Dr. Sinan KANDEMİR
Supervisor, Department of Mechanical Engineering,
İzmir Institute of Technology

Prof. Dr. M. İ. Can DEDE
Head of the Department of Mechanical Engineering

Prof. Dr. Mehtap EANES
Dean of the Graduate School

ACKNOWLEDGMENTS

I appreciate my intense respect and gratitude to my supervisor Assoc. Dr. Sinan KANDEMİR for his unwavering support and assistance throughout my thesis studies. His inspiration has been significant in my graduate education and life, and I will forever be grateful to him. I also want to thank Dr. Talha ERAZ for his valuable assistance and advices.

I am also thankful to TOTOMAK company and its employees; Oğuzcan ADIGÜZEL, Mehmet DONDURAN, Mehmetcan UYAN, Gökçe AKKUŞ, and Kurtuluş SUBAŞI for their valuable assistance. I also would like to thank my friend Mehmet Yalçın SIRMALILAR for his moral supports throughout my studies.

Lastly, I would like to thank my family members sincerely; my parents Murat ATASOY and Müjdet ATASOY, and my brothers Taner ATASOY and Mert ATASOY for their endless support, guidance, and love throughout my life. Their unconditional love and support have given me the strength to overcome challenges. In particular, I want to express my deepest love and appreciation to my mother who has been my guiding light, source of power, and greatest inspiration. Thank you mom for everything you have done for me.

ABSTRACT

MACHINABILITY INVESTIGATION OF RECYCLED SHORT CARBON FIBER REINFORCED MAGNESIUM MATRIX COMPOSITES

This study investigated the machinability of short carbon fiber reinforced magnesium matrix composites, which are considered to be novel materials. AZ91 alloy and its composites containing 2.5 and 5 wt.% recycled carbon fiber (rCF) reinforcements were used for machinability investigation. The samples were face milled using an uncoated carbide cutting tool under dry cutting conditions at different cutting speeds (480-560-640 m/min) and feed rates (0.65-0.8-0.95 mm/min). The experimental design was determined based on Taguchi L_9 (3^3) orthogonal array. The obtained results were analyzed via the Taguchi, ANOVA and regression methods. The study examined the surface roughness, cutting forces, possible wear formations on cutting inserts and chip morphology, which indicate machinability performance. The most promising machinability results in terms of the surface roughness and cutting force were obtained for AZ91 alloy, while the poorest performance was obtained for 5 wt.% rCF reinforced composite. It was concluded that the increase in reinforcement content led to increased surface roughness and cutting force. In addition, a significant BUL (built-up layer) formation on the cutting inserts was detected via SEM and EDX analyses. Based on the examination of chip morphology, spiral shaped continuous chips were predominantly generated in all experiments. The results showed that the composites were machinable, and the cutting parameters were suitable for future studies.

ÖZET

GERİ DÖNÜŞÜM KISA KARBON FİBER TAKVİYELİ MAGNEZYUM ESASLI KOMPOZİTLERİN TALAŞLI İŞLENEBİLİRLİĞİNİN ARAŞTIRILMASI

Bu çalışmada, yeni malzemeler olarak düşünülen kısa karbon fiber takviyeli magnezyum matrisli kompozitlerin işlenebilirliği araştırılmıştır. AZ91 alaşımı ve ağırlıkça %2,5 ve 5 oranında geri dönüşüm kısa karbon fiber (rCF) içeren kompozitleri çalışmada numune olarak kullanılmıştır. Numuneler, kuru kesme koşullarında, farklı kesme hızları (480-560-640 m/dak) ve ilerleme oranlarında (0.65-0.8-0.95 mm/dak) kaplamasız karbür kesici takım kullanılarak yüzey frezeleme işlemine tabi tutulmuştur. Deney tasarımı, Taguchi L_9 (3^3) ortogonal dizisine göre yapılmış olup elde edilen sonuçlar Taguchi, ANOVA ve regresyon analizi yöntemleri ile incelenmiştir. Çalışmada yüzey pürüzlülüğü, kesme kuvveti, aşınma fenomeni ve talaş formları işlenebilirlik açısından incelenmiştir. Yüzey pürüzlülüğü ve kesme kuvveti açısından en tatmin edici performans AZ91 alaşımının talaşlı işlenmesinde elde edilirken, en zayıf performans ağırlıkça %5 rCF takviyeli kompozit için elde edilmiştir. Bu duruma dayanarak takviye artışının artan yüzey pürüzlülüğü ve kesme kuvvetlerine neden olduğu sonucuna varılmıştır. Ayrıca kesici takımların SEM ve EDX analizi sonucunda önemli ölçüde YK (yığıntı katmanı) oluşumu tespit edilmiştir. İncelenen talaş formları sonucunda tüm deneylerde ağırlıklı olarak spiral şekilli sürekli talaş formları oluşmuştur. Çalışmanın sonunda kompozitlerin işlenebilir ve kesme parametrelerinin gelecek çalışmalar için uygun olduğu sonucuna varılmıştır.

TABLE OF CONTENTS

LIST OF FIGURES

Figure **Page**

Figure **Page**

Figure **Page**

LIST OF TABLES

CHAPTER 1

INTRODUCTION

There has been a concentration on creating metallic materials that are both lightweight and strong for various potential uses as the industry advances. Due to their low densities, aluminum (Al) and magnesium (Mg) alloys have become prevalent in numerous industrial applications. Their relatively improved specific strength (strength/density) makes them highly desirable for their use in applications where reducing weight is crucial, such manufacturing electronic frames, vehicles and aircraft structures. Mg as being the lightest available structural metal with a density of 1,74 g/cm^3 can be employed as an alternative choice to several denser conventional alloys. However, Mg alloys tend to exhibit relatively weak mechanical strength, low ductility and corrosion resistance. As a solution to this challenge, researchers have developed Mg matrix composites that are usually more costly to produce.

Researchers have recently focused on using recycled reinforcements to minimize the cost of composite manufacturing and contribute to sustainable manufacturing. The high demand for lightweight materials in engineering has prompted efforts to develop Mg matrix composites and low-cost fabrication techniques. Thus, Mg matrix composites have been produced with different production methods using various reinforcements, e.g. particles and fibers.

In order to obtain the desired dimensions after the production process, machining is usually required. Therefore, the machinability of a material is a crucial issue concerning industrial applications. The machinability of a material depends on microstructure, chemical composition, production methods and applied heat treatments. Although some materials exhibit similar mechanical properties, they may show different machinability characteristics due to differences between their chemical composition and microstructures. Thus, machinability studies are crucial to examine the machinability properties of a material.

The previously reported works suggest that the studies on Mg alloys and composites generally concentrate on subjects such as examining the microstructure, mechanical and physical properties. The lack of research on the machinability of Mg alloys and their composites has been the motivation of this study. Therefore, the

machinability of Mg matrix composites, which needs to be fully understood, was investigated in the study. The examination focused on surface roughness, cutting force, insert wear, and chip formation of the machined samples.

CHAPTER 2

LITERATURE REVIEW

Mg alloys, composites and their production methods, machining, and previous studies related to this work are outlined to provide a background in this chapter.

2.1. Mg and Its Alloys

Mg is a significant structural element used in aviation, maritime and automotive industries due to its low density and high recyclability properties. However, pure Mg has poor mechanical properties, and it is commonly alloyed with other elements, such as Al, Zn (zinc), and Mn (manganese), to enhance its properties.[1] The resulting alloys have different properties, such as relatively higher strength, finer castability and weldability, depending on the combination of alloying elements. Thus, the usage area of Mg alloys is gradually increasing. Al shaping is usually more effortless than the shaping of Mg due to the differences in their crystal structures.[2] Al has a face centered cubic (FCC) crystal structure. The FCC structure of Al provides a total of 12 slip systems that facilitate the shaping. On the other hand, Mg has a hexagonal close packed (HCP) crystal structure. The HCP structure of Mg offers 3 slip systems that limit the shaping of Mg. Hence, studies on Al are more comprehensive compared to studies on Mg.

The Mg-Al-Zn (AZ) ternary alloy system is one of the most widely used Mg alloy groups. The name "AZ" is derived from the chemical symbols of Al and Zn primary components. The manufacturing of AZ alloys is often accomplished by casting to produce components of different shapes and sizes. The composition of AZ alloys varies depending on their intended use, and their properties can be customized by adjusting the concentrations of alloying elements. AZ91 is a widely used commercial Mg cast alloy in the automobile and aviation industries thanks to its relatively high strength and castability properties.[3] It mainly contains 9 wt.% Al and 1 wt.% Zn. Al is the most commonly used alloying element in Mg alloys. It enhances strength, ductility, and castability of Mg alloys at temperatures generally below 120 °C. [3] Zn is mainly used to improve the corrosion resistance of Mg alloys.

2.2. Composite Materials

The progress of technology and modern industry largely relies on materials, and the limited performance of traditional materials prompts designers to explore novel materials. Consequently, the demand for novel materials is increasing for modern technological applications. Hence, new materials should be highly efficient and reliable. Materials must be light and resistant to challenging conditions such as high/low temperature, pressure, and high corrosion. In some cases, three main types of conventional materials (metals, ceramics and polymers) may not be sufficient to meet the desired requirements. As a result, a combination of materials was considered, and composite materials have emerged. The global composites market grew at an annual rate of about 8% from 1960 to 2010.[4] This ratio is expected to rise thanks to the increasing need for composite materials.

Composite materials are comprised of two or more distinct constituents. These constituents are combined to form a novel material with structural properties that cannot be found in any of these constituents. Composite materials are in high demand due to their lightness, durability, design flexibility, dimensional accuracy and long life.[5] As a result of these utilities, composite materials are extensively used in various industries, e.g. automotive, marine, aviation, robotics and biomedical.

An ordinary composite material comprises two phases: continuous and discontinuous. The continuous phase is the main component of composites and is called as the matrix phase. The discontinuous phase is the part that is embedded into the matrix. The dispersed (discontinuous) phase is usually surrounded by the matrix (continuous) phase. Composites are generally classified into three main groups according to their matrix types: metal, ceramic and polymer matrix composites. Composites are also classified according to the types of reinforcement elements: fiber reinforced, particle reinforced, and structural composites. The classification of composites is shown in Figure 1.

Polymer matrix composites (PMCs) are widely used in composite applications because of their low density and high resistance to wear and corrosion.[6] The significant disadvantages of PMCs are their low thermal resistance property. Therefore, they are not preferred as building materials in applications requiring elevated temperatures. Ceramic matrix composites (CMCs) are used due to their high strength, chemical stability and

wear resistance properties at elevated temperatures.[7] However, the low fracture toughness property of CMCs limits their use.

This study is primarily concerned with metal matrix composites (MMCs). Therefore, the following sections provide information about MMCs, their properties, and production processes.

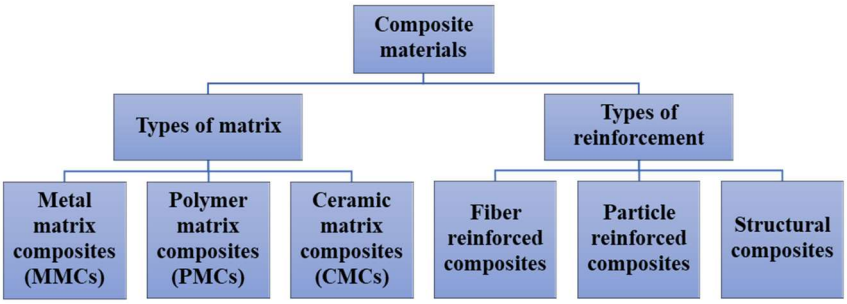

Figure 1. Classification of composites based on matrix and reinforcement types

2.2.1. Metal Matrix Composites (MMCs)

MMCs are preferred in many engineering applications since they outperform PMCs due to their improved high temperature mechanical and physical properties.[8] These properties include higher hardness and strength, and electrical and thermal conductivity values.

MMCs consist of at least one reinforcement material, such as ceramic particles, fibers, or whiskers, as illustrated in Figure 2. The function of these materials is to enhance the properties of a relatively soft metal matrix.[9] The matrix in an MMC generally serves as the primary structural component that allows the transmission and distribution of any applied force to the reinforcement phase via the interfacial bond.[10] The composition of the two materials results in a composite material with superior properties compared to monolithic materials.

Furthermore, fibers are a remarkable reinforcement for MMCs as they improve anisotropy properties.[11] Fiber reinforced (FR) MMCs combine the strength and stiffness of the fibers with the toughness and ductility of a metallic matrix. Carbon fibers are in demand in FR-MMCs in lightweight applications due to their low density. Even though FR-MMCs possess numerous benefits, they also have certain constraints. For instance, their production can be complex and costly, and the fibers may be susceptible to damage during handling and processing.[12]

One of the main objectives of composite production is cost reduction, as it is generally more expensive than conventional alloy production. Using rCFs is a viable option to achieve this goal since they are widely available in the market.[13]

Recycled and virgin carbon fibers (vCFs) differ in mechanical properties and environmental impact. The vCFs generally have higher strength than rCFs due to the recycling process resulting in some degradation of the carbon fiber strips, thus reduced mechanical performance.[14] However, recycling technologies are continuously improved, narrowing the performance gap with vCF. Recycling CF is more sustainable than producing vCF, which involves energy-intensive processes and emits greenhouse gases.[15,16] Therefore, the demand for rCFs is increasing as sustainability becomes a priority in automotive, aerospace, and wind energy industries. The production of vCF is complex and requires specialized equipment, resulting in high costs. However, recycling CF offers cost reduction by 20-40% using waste PMCs.[17] Furthermore, the composition and manufacturing process of MMCs can be customized to meet specific requirements.

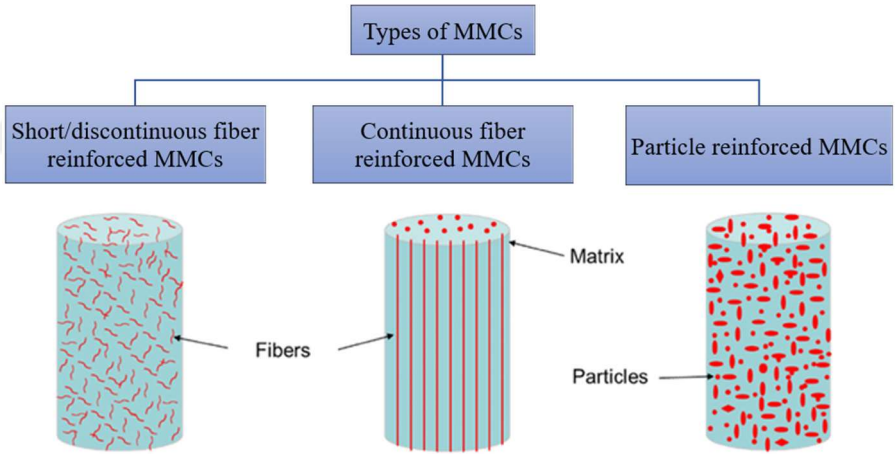

Figure 2. Schematic classification of MMCs based on reinforcement type[18]

2.2.2. Production Methods of MMCs

Due to the diversity of utilized matrices and reinforcements, a range of techniques have emerged in the production of MMCs. The selection of composite material production methods involves considering factors such as matrix and reinforcement material and type, desired mechanical and physical properties, part shape, and cost. Two main categories for creating composite materials are solid state and liquid state production methods.

The solid state production method of MMCs involves consolidating metal powders and reinforcements at high pressure and temperature.[19] This method uses a matrix material in powder form and reinforcements in fiber or particle form. Different compaction techniques, such as powder metallurgy, hot pressing, or extrusion, consolidate the matrix and reinforcement. Once compacted, the material undergoes additional heat treatment to enhance the bonding between the matrix and reinforcement. Solid state production is preferred for creating high strength composites with more uniform reinforcement distribution and improved mechanical properties.[20] However, it is usually more costly for mass production compared to the liquid state production methods.

Liquid state production methods such as stir casting, squeeze casting, and infiltration are commonly utilized for MMCs. The squeeze casting process involves pouring molten metal into a preheated mold.[19] The reinforcement material is usually inserted into the mold before the molten metal is poured. High pressure is then applied to consolidate the material. The infiltration method involves placing the reinforcement material in a mold and injecting the molten matrix material under pressure. The reinforcement material is usually in the form of a preform or porous material. The resulting composites have relatively high mechanical properties in the infiltration method.[20] However, it is usually more costly than stir and squeeze casting.

2.2.2.1. Stir Casting

This section describes the stir casting technique used to fabricate the composites for this work.

The stir casting is a widely used method in the production of MMCs.[21] In this process, a rotating impeller is employed to stir molten matrix and reinforcement in a crucible, as shown in Figure 3. The impeller creates turbulence and vortex in the melt, which facilitates the distribution of reinforcement and enhances its dispersion throughout the matrix.[22] After stirring, the mixture is poured into a suitable mold for solidification into a desired shape. Consequently, a composite with a uniform dispersion of reinforcement and enhanced mechanical properties is produced.

The stir casting has several advantages, including its versatility and ease of use. This process can be adapted based on production requirements and is compatible with a wide range of matrix and reinforcement materials.

Despite its advantages, stir casting also has some limitations. One of these limitations is the risk of agglomeration or clusters of reinforcement [23]. This situation leads to a reduction in the mechanical properties of composite materials. Additionally, porosity in the composite may occur during the stir casting process due to trapped gas bubbles [24]. As a result of soluble gases, this problem can be addressed by optimizing the casting conditions.

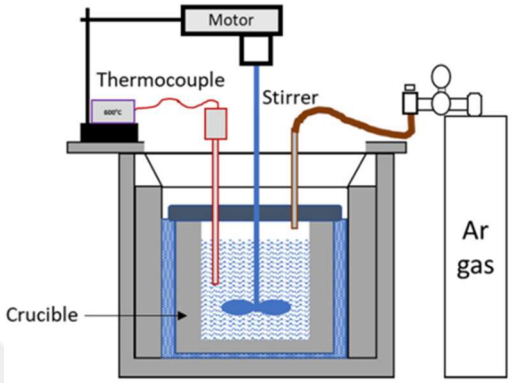

Figure 3. Illustration of stir casting method[25]

One crucial aspect to consider when producing cast MMCs is the bonding between matrix and reinforcement, known as wettability. Adequate wetting is critical in achieving a strong and durable bond between the matrix and reinforcement in composite production. It enables the molten matrix to fully envelop and adhere to the reinforcement, ensuring a uniform distribution throughout the composite.[26] To achieve effective wetting, the contact angle (θ) between the liquid and the solid surface is mostly less than 90°.[27] A higher contact angle leads to low wetting or no wetting, as shown in Figure 4. Without adequate wettability, molten matrix cannot adhere to reinforcement, leading to reinforcement clustering in the melt.[28] Therefore, ensuring adequate wettability is essential for producing high quality composite materials with optimal performance.

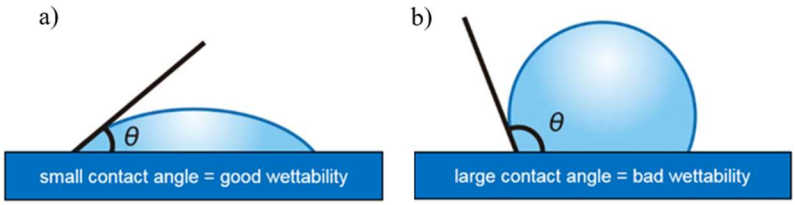

Figure 4. Illustration of wettability phenomena based on contact angle: a) small contact angle, b) large contact angle[29]

2.3. Machining

The main aim of manufacturing processes is to convert raw materials into a final product that is distinct and unique in its characteristics, features, and functionality. Various production techniques are employed to achieve the desired final products. These manufacturing techniques are categorized into two main groups: machining and chipless manufacturing.[30] These techniques exhibit dissimilarities in their methodologies and applications. Additionally, the application areas for each manufacturing method change depending on the requirements of final products and the characteristics of workpiece materials. Machining methods include the removal of chips from raw material during the processing of the workpiece. On the other hand, chipless manufacturing methods, e.g. welding, casting and forging, do not involve removing any chips from the raw material.

Machining is vital for industrial manufacturing and is typically required, followed by casting. This production method requires specialized tools such as lathes, drills, and milling cutters to remove excess material from a workpiece as chips. This procedure aims to achieve the desired dimensional accuracy and surface quality of the workpiece, ensuring that it meets the required specifications for the final product. Machining processes are generally utilized to finalize the materials produced by casting, forging, rolling and other chipless manufacturing methods. Numerous products undergo machining in various essential industrial fields such as aerospace, automotive, and maritime to achieve their ultimate tolerances.

Using improper cutting parameters in machining can quickly make the cutting tools unusable due to breakage, rapid wear, and deformation. This situation leads to economic losses, deterioration of workpiece dimensions, and inadequate surface quality, which may require a second operation.[31]

The machining parameters significantly govern a machining process. The most influential machining parameters include the following:

- **Cutting speed:** It is the rotational speed of the cutting tool or workpiece and is highly dependent on the characteristics of the workpiece.
- **Feed rate:** It refers to the distance the tool travels on a workpiece during one spindle rotation.
- **Depth of cutting:** It is the penetration depth of the cutting tool into the workpiece. Lower cutting speeds, feed rates and depths of cut are usually suggested for

relatively hard materials to obtain more efficient machinability performance, unlike soft materials. The main cutting parameters are illustrated in Figure 5.

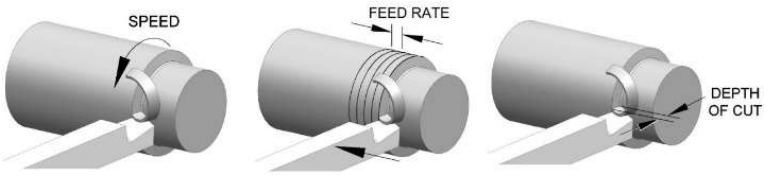

Figure 5. Illustration of main cutting parameters in turning operation[32]

Improving *machinability* is a vital goal for the machining industry. It refers to the ease of shaping a workpiece using a cutting tool to achieve the desired shape.[33] The most common criteria to evaluate the machinability performance of materials are as follows:

- **Surface quality:** It refers to the smoothness, accuracy, and consistency of the surface finish of the machined workpiece. Relative better machinability usually results in a higher surface finish quality that provides the necessary specifications.
- **Cutting forces:** High cutting forces are undesirable as they increase tool wear and energy consumption. In addition, increasing cutting forces may increase the vibration on the cutting tool and workpiece, leading to a poorer surface finish.[34]
- **Cutting tool life:** A better machinability process tends to extend the lifespan of cutting tools, reducing costs and increasing efficiency.[35]
- **Chip formation:** Long chips usually increase the surface roughness of the workpiece and are not desired for machining due to difficulties in evacuating them.[36]

2.3.1. Mechanics of Machining and Chip Formation

The geometry of machining operations is usually complex. A simplified cutting model has been developed due to the complexity of the machining operations. This model is known as orthogonal cutting. It ignores complexities and describes the mechanics of the operation quite well.[37] An actual machining operation is three dimensional, but the orthogonal model only considers two dimensions for analysis. The orthogonal cutting employs a wedge-shaped tool with a cutting edge perpendicularly to the cutting speed direction. As the tool is forced into the workpiece, the chip is generated through shear deformation along the shear plane, as shown in Figure 6.

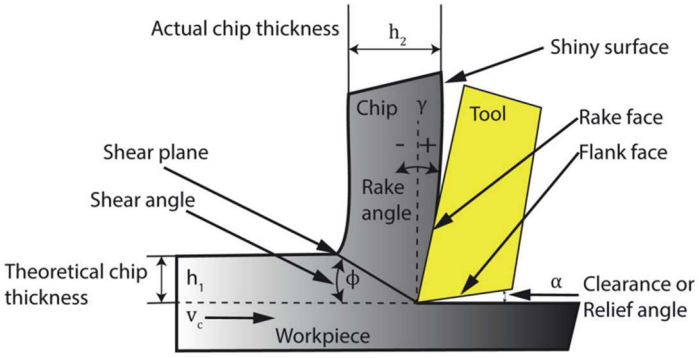

Figure 6. Orthogonal cutting model[38]

Figure 7(a) illustrates the forces acting on the chip during orthogonal cutting. The tool acts two perpendicular forces on the chip: friction force (F) and normal force to friction (N). F acts in opposition to the chip flow across the rake face of the tool. N is perpendicular to F. Apart from the tool forces acting on the chip, there are two components of forces acting on the chip by the workpiece: shear force (F_s) and normal force to shear (F_n). The cutting (F_c) and thrust force (F_t) acting on the tool are shown in Figure 7(b). F_c is in the direction of the cutting, the same direction as the cutting speed, and is perpendicular to the F_t. Since the application directions of F, N, F_s and F_n force components vary according to the tool geometry and cutting conditions, they cannot be measured directly in machining.[39] However, a dynamometer or load cell can measure the resultant force (R") of F_c and F_t acting on the cutting tool.

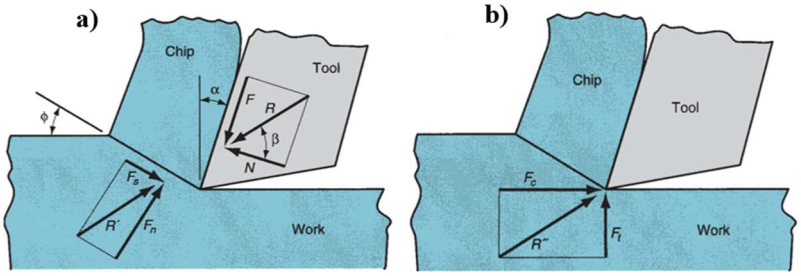

Figure 7. Forces in orthogonal cutting: a) acting on the chip, b) acting on the tool[39]

There are three common chip types classified based on their form in metal machining, as shown in Figure 8:

- **Continuous chip:** It is usually formed in machining ductile materials at higher cutting speeds, relatively low feed rates and depths of cut. A better surface finish is usually achieved as this chip type is generated.[40] However, it tends to increase

the surface roughness at longer machining cycles due to difficulties in its evacuation.[41]

- **Discontinuous chip:** It is usually generated in machining brittle materials at low cutting speeds. The chips are usually formed in separate segments, resulting in an irregular surface finish.[39] Higher tool-chip friction, feed rates, and cutting depths increase the formation of this chip type.
- **Serrated chip:** This chip type has a saw-tooth appearance due to cyclical chip formation of high and low shear strain. It is common in machining difficult-to-machine metals, such as titanium (Ti) alloys and nickel (Ni) base superalloys.[42]

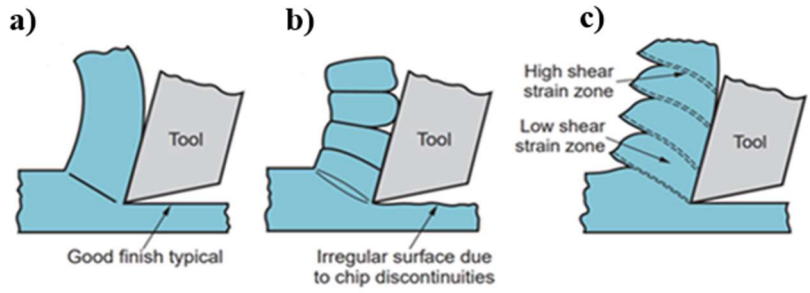

Figure 8. Common chip forms: a) continuous chip, b) discontinuous chip, c) serrated chip[39]

2.3.2. Machining Processes

The most widely used machining methods in the metal industry are turning, milling, and drilling, as illustrated in Figure 9.

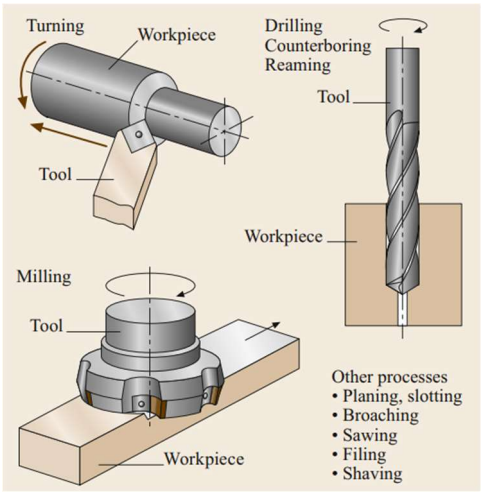

Figure 9. Illustration of common machining processes [43]

These processes are not only limited to metals, they can also be employed for machining polymers and composites.[44] Since the machining method employed in the study is face milling, this method is scrutinized in the following section.

2.3.2.1. Face Milling

Face milling involves using a rotating tool (milling cutter) to remove chips from the workpiece, as illustrated in Figure 10. The cutter employs cutting inserts. The cutter rotates perpendicular to surface of the workpiece while moving parallel. A face milling cutter with varying sizes and teeth is used based on dimensions of the workpiece and cutting conditions, as seen in Figure 11. Different inserts available for various workpieces and desired final products are shown in Figure 12.

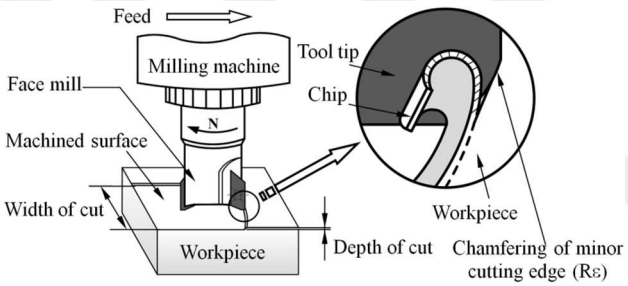

Figure 10. Illustration of face milling method[45]

Figure 11. Types of face milling cutters[46]

Figure 12. Types of face milling inserts[47]

Wear formation on the cutting inserts is a crucial issue as it provides insight into machinability performance. Common wear types on the inserts are illustrated in Figure 13. They are as follows:

- **Crater wear:** It occurs on the rake face of the cutting insert due to the high temperatures and mechanical forces generated during machining.[48]
- **Flank wear:** It is a common wear type that occurs in machining hard materials at high cutting speeds and feed rates.[49]
- **Notch wear:** It is characterized by the presence of small notches along a cutting edge, resulting from the combined effects of friction and elevated temperatures.[50]
- **Thermal cracks and plastic deformation:** Elevated temperatures can cause thermal cracks and plastic deformation (permanent distortion).[51] Instantaneous temperature changes lead to an increase in the formation of thermal cracks.[52]
- **BUE and BUL:** Built-up edge (BUE) is a common phenomenon in machining ductile materials, where some workpiece materials adhere to the cutting edge of the insert due to increasing cutting temperature and stress, as shown in Figure 14. These adhered materials form a layer on the rake face of the insert over time, referred to as a built-up layer (BUL). [53]

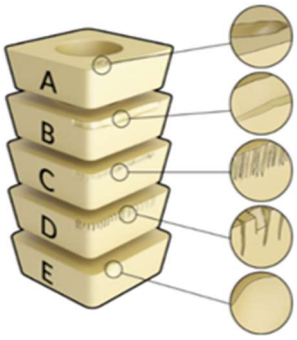

Figure 13. Common wears in machining: a) crater wear, b) flank wear, c) notch wear, d) thermal cracks, e) plastic deformation[54]

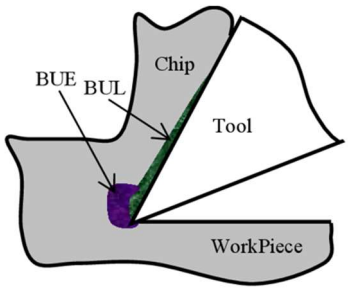

Figure 14. Illustration of BUE and BUL [55]

2.3.3. Machining of Mg Alloys and MMCs

This section reports the previous machining studies in the literature on Mg alloys and MMCs.

Surya et al.[56] investigated the influence of grain refinement on the machining of AZ91 alloy. The authors subjected the alloy to friction stir processing (FSP) for grain refinement. Drilling experiments were conducted on both FSPed AZ91 alloy (21.7±13.5 μm) and as-cast AZ91 (166.5±8.7 μm) alloy under different cutting speeds (90-355 r/min) and feed rates (14-26 mm/min). During the drilling of FSPed AZ91 alloy, around 30% higher mean cutting forces were observed than AZ91 alloy. The authors attributed this result to the increased hardness of the material due to grain refinement. The optical microscope examination revealed that the FSPed AZ91 alloy exhibited better surface quality. The study concluded that although grain refinement increases cutting force, it enhances surface quality in drilling.

Akyuz[57] examined the machinability of AZ series Mg alloys (with 1 wt.% Zn). The alloys were turned under dry cutting conditions at different speeds (56-168 m/min) and feed rates (0.068-0.204 mm/rev). The cutting forces were measured, and insert investigations were conducted. BUE formations that increased with increasing Al content were observed. Cutting forces increased as the Al content increased (1 to 9 wt.%), were attributed to BUE formation during turning. A direct proportionality was found between the increase in Al content and cutting forces.

Dinesh et al.[58] investigated the effects of cryogenic cooling and dry cutting conditions on the machining of ZK60 Mg alloys. The study examined cutting temperature, forces, and surface roughness under various cutting speeds (60-120 m/min) and feed rates (0.1 and 0.15 mm/rev). Cryogenic cooling resulted in a reduction in cutting temperature compared to dry cutting conditions. Dry machining conditions led to a decrease in cutting forces with increasing cutting speed. In contrast, cutting forces decreased with increasing cutting speed under cryogenic cutting conditions up to 90 m/min. However, after 90 m/min cutting speed, the cutting forces increased with sudden cooling and work hardening. Surface roughness decreased under cryogenic conditions compared to dry cutting conditions.

Shi et al.[59] researched the impacts of high speed milling of Mg alloys on a cemented carbide insert under dry cutting conditions. The AZ91D alloy was milled at

1600-2000 m/min cutting speeds, with a constant cutting depth and feed rate. At high cutting speeds, a flank build-up commonly covered the flank face of the insert. Intense flaking was dominant at 1600 m/min cutting speed, while significant flank wear and fractures were observed at 1800 and 2000 m/min cutting speeds. The increasing cutting speed led to surface roughness increase. The intermittent chip morphology, typical in the study, was attributed to wear and deterioration of the cutting tools.

Hou et al.[45] investigated the chip ignition in machining Mg alloys. AZ91D and AM50A were face milled under dry machining conditions and different cutting parameters (251-1257 m/min of cutting speeds, 5-40 µm of cutting depths, and constant 400 mm/min of feed rates). Undesirable formations such as sparks, ignition and flashing during machining were recorded. Unlike lower and higher cutting speeds and feed rates, it was observed in both alloys that spark, flash and ignition occurred intensely at medium cutting speeds (750-800 m/min) and depths of cut (20-40 µm). The study demonstrated that AZ91D was more flammable than AM50A alloy under dry milling conditions.

Hereafter, the machinability studies of MMCs in the literature are covered within the scope of the study.

Chou and Liu[60] conducted a study to examine the effect of CVD (chemical vapor deposition) coated diamond cutting tools in machining MMCs. Al359/SiC (silicon carbide) with 20 wt.% MMC was chosen as the sample. The samples were turned on a CNC machine using at various machining parameters (1-6 m/s of cutting speed, 0.005-0.3 mm/rev of feed rate, and 1-2 mm of cutting depth). Temperature rise and wear rate on the insert were measured. The study found that the feed rate is the most critical factor affecting insert wear and temperature rise at the insert tip. Increasing the feed rate led to an increase in tool wear and cutting temperature.

Devaraj et al.[61] investigated the effects of micro-textured tool design parameters on machinability. They used micro-holed inserts with different hole diameters (100-200 µm) and depths (80-200 µm) to machine Al6061/SiC (7 wt.%) composite material on a CNC lathe. Surface roughness was measured, and it was found that an insert with a 200 µm hole diameter and 140 µm hole depth provided the most promising surface roughness results. Hole diameter was found to be a more effective parameter than hole depth, which enhances surface roughness.

Venkatesh et al.[62] conducted a study on the performance of PCD (polycrystalline diamond) cutting tools in machining A356/SiC 20 wt.% composite. The samples were turned using a PCD 1300 grade tool under dry cutting conditions with varying cutting

parameters (100-600 m/min cutting speed, 0.108 and 0.2 mm/rev feed rate, and 0.25-0.75 mm cutting depth) for tool wear investigation. The results showed that the MRR increased from 100 to 535 mm^3/min at higher cutting speeds and feed rates. However, tool wear also increased significantly at higher cutting speeds and feed rates due to the high content of SiC particles. The study concluded that the PCD 1300 grade tool is unsuitable for machining the composite.

Bachchhav and Naranje[63] investigated the influence of aluminum oxide particles (Al_2O_3) volume fraction on the machinability of Al-Al_2O_3/10-50 wt.% in electro discharge machining (EDM). The study examined the surface roughness and material removal rate (MRR) of MMCs. The results showed that increasing the reinforcement ratio decreased the MRR by around 43% while increasing the current (5-15 I), voltage (30-70 V), and pulse time (11-55 μ sec) increased the MRR by around 30%. Increased Al_2O_3 concentration, current, voltage, and pulse time also led to poorer surface roughness.

Manna et al.[64] compared experimental and theoretical results for improving surface quality in machining Al/SiC composites. The study involved subjecting the samples (LM25-SiC/10 wt.%) to a turning process under dry cutting conditions using different cutting parameters according to Taguchi L_{27} orthogonal array. The authors developed a theoretical model by analyzing the ANOVA results. The experimental study revealed that increased feed rate (0.16-0.48 mm/rev) and depth of cut (0.5-1 mm) resulted in higher Ra values, while increased cutting speed (40-160 m/min) resulted in better surface performance. The difference between the developed theoretical model and experimental results ranged from around 3.6% to 10%.

Balasubramanian et al.[65] investigated the machinability of AZ91D/SiC (3, 6 and 9 wt.%) composites manufactured by the squeeze casting method. The effect of reinforcement content on the machinability of AZ91 alloy was investigated. The specimens were turned on a CNC lathe, and the surface roughness of them was measured. It was revealed that Ra values decreased as the reinforcement content increased. Additionally, it was observed that the MRR increased with an increase in cutting speed and feed rate.

Pedersen et al.[66] analyzed the machinability of Mg matrix composites reinforced with SiC particles using carbide inserts. The study involved milling ZK60A-T5/SiC (20% vol.) composite using a PVD coated carbide insert at varying cutting parameters. The study highlighted that increasing the cutting depth and feed rate led to increased flank wear, which resulted in poor surface roughness.

In the literature survey, it has been observed that studies on the machinability of Mg matrix composites are rare compared to Mg alloys and Al matrix composites, and particles were commonly embedded into matrices in the composites. Therefore, it is considered that there is a gap in the literature. Hence, this study concentrated on the machinability of carbon fiber reinforced Mg matrix composites.

CHAPTER 3

EXPERIMENTAL PROCEDURES

This chapter mentions the properties of the samples and their production process, the experimental design and process, and the devices used in the study.

3.1. Materials

AZ91 alloy and its composites containing 2.5 and 5 wt.% rCF were used in the study. These samples were previously used in the study of Kandemir et al[67]. The chemical composition of the AZ91 reference alloy as the matrix material is given in Table 1. The properties of rCFs as reinforcement are shown in Table 2. The rCFs were produced by recycling from waste PMCs and were supplied from CarboNXT GmbH.

Table 1. Chemical composition of the reference alloy (wt. %)[67]

Mg	Al	Zn	Mn	Nd	Si	Ca	Cu	Fe
Bal.	8.73	0.67	0.21	0.019	0.019	0.0014	0.0027	0.0013

Table 2. Properties of rCFs from PMCs[67]

Carbon fiber content	95%
Tensile strength	>3500 MPa
Tensile modulus	>230 MPa
Fiber diameter	6 μm (±1μm)
Density	1.83 g/cm^3
Sizing content	0%
Average fiber length	500 μm

3.2. Composite Fabrication

The samples were manufactured by casting technique under an inert gas (Ar/1% SF_6) by adding Al foil bags containing 2.5 and 5 wt.% rCFs to the commercial AZ91 molten alloy at 710 °C. The reason for adding rCFs in Al foil bags is to prevent undesirable releases during manufacturing.

During the stirring process, the high shear dispersion (HSD) technique was employed to the melt to ensure the homogeneous distribution of rCFs and prevent or minimize possible agglomeration of fibers in the melt. The principle behind the operation of the HSD device involves shearing the melt drawn into the stator and pushed back through the stator openings, as illustrated in Figure 15. The HSD device (preheated to 350 °C) was utilized to shear the alloy at 2000 rev/min for 5 minutes. Compared to mechanical mixers, the HSD device is recognized for its superior ability to disperse particles or fibers that may agglomerate, and it has been observed to provide efficient results in the studies.[68,69]

Once the dispersion process was completed, the composite slurry was transferred into cylindrical steel molds. The molds were then moved at a 100 mm/minute rate and subsequently submerged in a water bath while maintaining controlled solidification conditions. The reference alloy and composites were produced under the same casting conditions. As a result, AZ91 alloy, AZ91/2.5 and 5 wt.% rCF reinforced composite samples used in the study were obtained. The dimensions of cast ingots vary in different sizes, with a diameter of around 108 mm and a height of around 150-180 mm. Table 3 provides the hardness and density values obtained from the samples.

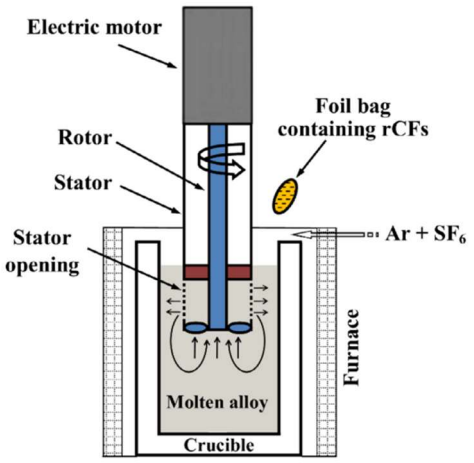

Figure 15. Illustration of HSD process[67]

Table 3. Hardness and density properties of specimens[67]

Material	Hardness (HV)	Density (g/cm^3)
AZ91	55.5 ± 2.9	1.818
AZ91/2.5 wt.% rCF	59.9 ± 2.2	1.817
AZ91/5 wt.% rCF	61.1 ± 4.2	1.804

3.3. Design of Experiment

Experimental design improves the process by identifying the variables that significantly influence the process and optimizing them for the desired results. This approach shortens the processes and saves costs. A full factorial experimental design can be difficult in experimental studies as it requires a large number of experiments, resulting in longer time and high cost.[70] Taguchi, Box-Behnken and Surface-centered composite experimental design methods have been used as an alternative to the full factorial experimental design in studies.[71–73] The Taguchi method was chosen as the experimental design method due to the limited number of the custom-made specimens used in the study. It aims to obtain experimental results by conducting fewer experiments. Thus, the Taguchi is an industrially practical and versatile method for optimizing parameters in studies.

Obtained results are evaluated by converting them to the S/N (signal/noise) ratio in the Taguchi method. The S indicates the measured values in the process, while N represents the undesired factors (noises) in the measured values. The S/N ratio is calculated and analyzed using various approaches. The approaches include: i) smaller is better, ii) larger is better, and iii) nominal is better. Equations 3.1-3.3 are used to calculate S/N ratios based on the approaches. In the equations, y refers to the output values, n indicates the number of y values and s refers to the standard deviation of y values. In any case, a higher S/N ratio is better. Therefore, the highest S/N ratio values indicate the most promising performance for the factors.[74] Therefore, the Taguchi method can determine optimum levels of factors.

$$\frac{S}{N}: \ -10 \ log \ (\frac{1}{n} \sum_{i:1}^{n} {y_i}^2) \ (smaller \ is \ better) \tag{3.1}$$

$$\frac{S}{N}: \ -10 \ log \ (\frac{1}{n} \sum_{i:1}^{n} \frac{1}{{y_i}^2}) \ (larger \ is \ better) \tag{3.2}$$

$$\frac{S}{N}: 10 \ log \left(\frac{\bar{y}}{s_y^2}\right) (nominal \ is \ better) \tag{3.3}$$

In addition to the Taguchi method, the effect rate of the factors that influence the outputs is statistically revealed by the analysis of variance (ANOVA).[75] The probability (p) value is usually used for interpreting the ANOVA results, and it is a measure that determines the statistical significance of the factors. A p-value less than 0.05 indicates that the factor is statistically significant and remarkably influences the dependent variable.[76] The regression coefficient (R-sq) is the other measure to interpret the ANOVA results. It reveals the rate of relationship between the variables. The R-sq values are always between 0 and 1 (100%). Higher R-sq values are better as they indicate the relatively better relation between the variables and the reliability of the ANOVA results.[77]

Furthermore, regression analysis is one of the methods used to analyze experimental results. Regression analysis is the mathematical expression of the relationship between dependent and independent variables.[78] It generates equations for experimental studies based on data. Therefore, regression equations help to obtain estimated results without experimentation and can be used to validate experimental results. The R-sq value indicates the accuracy and prediction success of a model in the regression analysis. A higher R-sq value indicates more accurate predictions in the regression analysis.[79]

Taguchi experimental design, ANOVA and regression analysis were conducted using the Minitab statistical software (Minitab 21). The first step in the process is to identify the factors (parameters) and their levels and then select the appropriate orthogonal array based on them. In this study, the selected factors are material (rCF content), cutting speed, and feed rate (table feed). The cutting depth is kept constant since the number of experiments rises based on the increasing number of parameters. The L_9 (3^3) orthogonal array was chosen based on the selected parameters. Table 4 shows the factors and their levels. The levels of the factors were determined based on the characteristics of the WC (tungsten carbide) cutting insert.

Table 4. Factors and their levels in the experimental design

Factors	**Unit**	**Level 1**	**Level 2**	**Level 3**
Material	-	AZ91 alloy	AZ91/2.5 wt.% rCF	AZ91/5 wt.% rCF
Cutting velocity (V_c)	m/min	480	560	640
Feed rate (V_f)	mm/min	0.65	0.80	0.95
Depth of cutting (a_p)	mm	1	1	1
Cutting insert	-	Uncoated WC insert	Uncoated WC insert	Uncoated WC insert
Machining medium	-	Dry	Dry	Dry

Considering the factors and levels in this research, 27 (3^3) experiments are normally required as the full factorial experimental design. However, the Taguchi method reduced the number of experiments to 9, as shown in Table 5.

Table 5. Experimental plan based on the L_9 orthogonal array

Exp. No.	Material	V_c (m/min)	V_f (mm/min)
1	AZ91	480	0.65
2	AZ91	560	0.80
3	AZ91	640	0.95
4	AZ91/2.5 wt.% rCF	480	0.80
5	AZ91/2.5 wt.% rCF	560	0.95
6	AZ91/2.5 wt.% rCF	640	0.65
7	AZ91/5 wt.% rCF	480	0.95
8	AZ91/5 wt.% rCF	560	0.65
9	AZ91/5 wt.% rCF	640	0.80

3.4. Experimental Setup and Process

The experimental setup for machining is shown in Figure 16. The setup consists of a CNC milling machine, a compression load cell, and a computer with a software system. As the samples used in the study were cylindrical blocks, the face milling was considered to be the most suitable operation for machining. The experiments were conducted on a CNC (computer numerical control) vertical machining device, as shown in Figure 17.

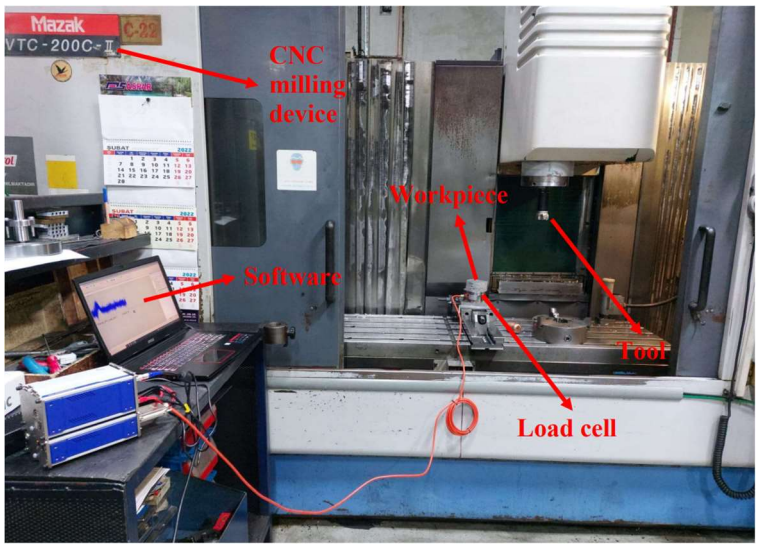

Figure 16. Experimental setup of the study

Figure 17. VTC-200C II / Yamazaki Mazak vertical machining device available in TOTOMAK company

The specimens to be machined were first drilled to attach the load cell via a fixture prior to the experiments, as shown in Figure 18(a). The load cell setup to measure cutting forces is shown in Figure 18(b). The forces generated in the face milling operation are illustrated in Figure 19. Cutting force (F_c) was measured via the load cell in the study.

The working principle of the load cell is based on receiving the force applied to the load cell as an electrical quantity and converting it into a force magnitude. The load cell structure consists of a metal body called a spring element and a Wheatstone bridge installed with strain gauges. When force is applied to the spring element, a displacement occurs on the load cell body. This displacement in the spring element is first detected via strain gauges as an impedance change and, an electrical signal is generated as an output over the whetstone bridge (circuit). This resulting signal is processed on a microprocessor as force or weight data. This resulting signal is processed on a microprocessor as force or weight data.

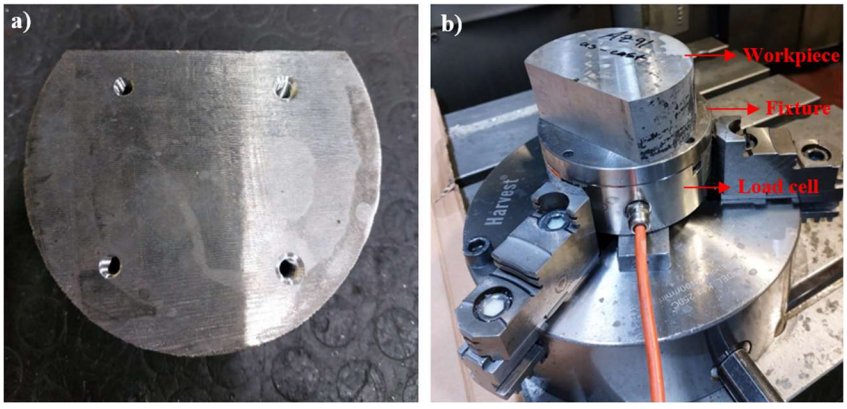

Figure 18. Cutting force measurement: a) prepared specimen to attach the load cell b) load cell setup

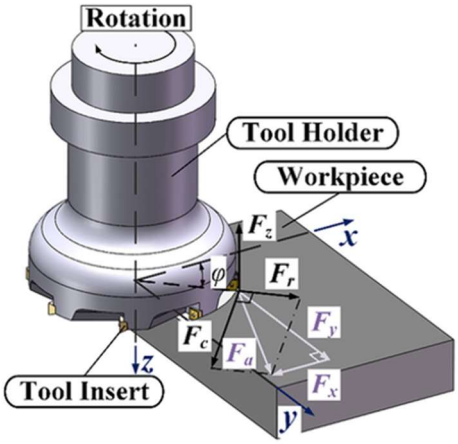

Figure 19. Components of the cutting force in face milling[80]

After the load cell setup installation, an uncoated WC insert was preferred because of its high strength, toughness, and ability to enhance efficiency in machining. The reason for using the uncoated insert is to examine possible wear scars on them. A 5-tooth milling cutter suitable for the insert was selected based on the size of the samples. The new edge of the inserts was used for each experiment in the study.

Each machining experiment was repeated three times, and instruments/devices were calibrated at the end of each experiment. The surface roughness of the samples was measured after the third repeat with a roughness measurement device available in TOTOMAK company, as shown in Figure 20.

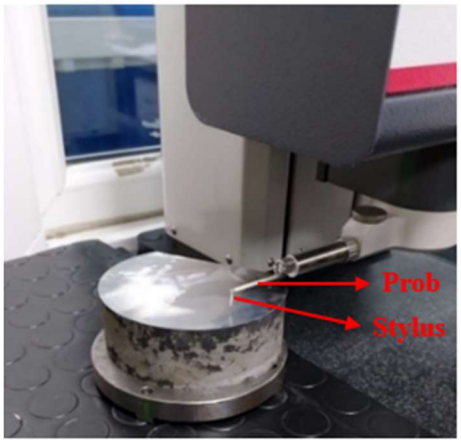

Figure 20. Surface roughness measurement

In this work, Ra surface roughness profile of the machined surfaces was measured. The Ra is a widely accepted roughness parameter that is calculated as the average of absolute values of coordinates through the roughness profile, as illustrated in Figure 21.

Two different spindle cutting textures were formed on the surfaces of samples depending on the spindle movement. Four roughness measurements in total were made on the surface textures for each sample.

Furthermore, the chips were collected after each experiment to examine the chip form. Finally, the cutting inserts were examined to detect possible wear via a universal SEM available in the IZTECH-Integrated Research Center (IRC).

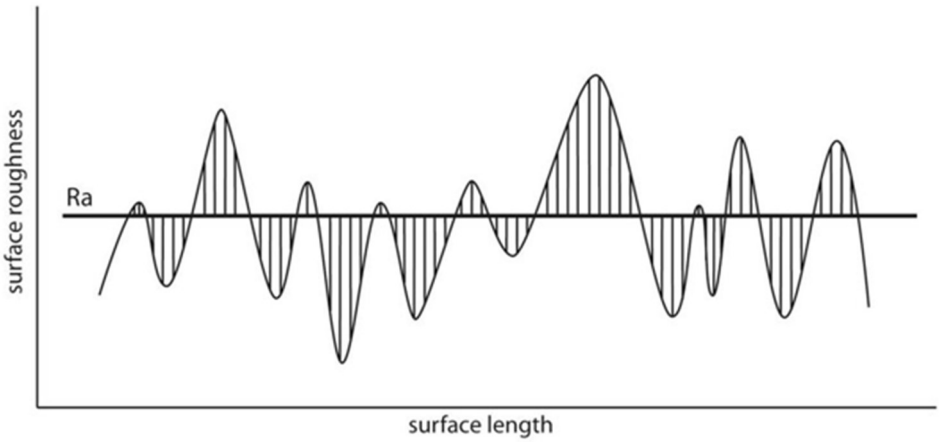

Figure 21. Ra surface roughness profile[81]

3.5. Experimental Instruments and Devices

This section outlines the specifications of the devices and instruments employed in the study.

3.5.1. CNC Milling Machine

The CNC machine used in the study allows 3, 4 and 5-axis machining and the spindle speed of the device can reach 12000 rpm. Table 6 depicts the technical specifications of the machine.

Table 6. Technical properties of the CNC machine

Table length (mm)	X/Y/Z axis movement (mm)	X/Y/Z rapid transverse (m/min)	Spindle motor power (kW)
2000 X 510	1660/510/510	36/36/36	18.5

3.5.2. Load Cell

The HT2 series compression load cell used in the study is shown in Figure 22. The load cell is resistant to off-axis loads and allows the measurement of loads up to 2 tons.

Figure 22. HT2 series load cell[82]

3.5.3. Cutting Insert

The technical dimensions of the double-sided insert with a total of eight cutting edges used in the study are shown in Figure 23. The double-sided insert provides cost savings compared to conventional single-sided inserts. The machining operation ranges recommended by the manufacturer for the cutting insert can be seen in Table 7.

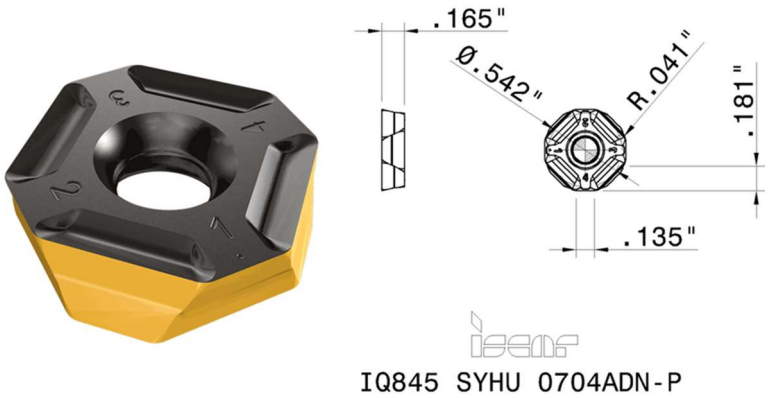

Figure 23. Technical dimensions of the milling insert[83]

Table 7. Recommended machining ranges of the cutting insert

Cutting speed (V_c)	Feed rate (f_z)	Depth of cutting (a_p)
100-600 m/min	0.10-0.25 mm/tooth	1-4 mm

3.5.4. Face Milling Cutter

Technical dimensions of the milling cutter suitable for double-sided inserts is shown in Figure 24.

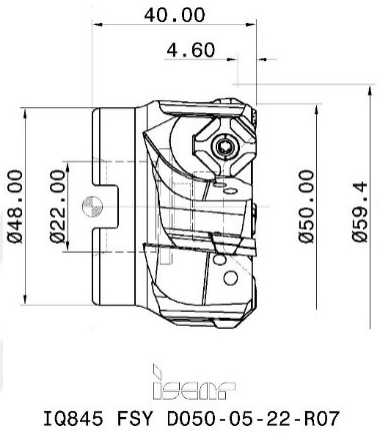

Figure 24. Technical dimensions of the milling cutter[84]

3.5.5. Surface Roughness Measurement Device

Marsurf GD 140 surface roughness measuring device is shown in Figure 25. In addition to surface roughness measurements, the device can make profile and waviness measurements.

Figure 25. MarSurf GD 140 surface roughness measurement device[85]

3.5.6. Scanning Electron Microscope (SEM)

FEI QUANTA 250 FEG model SEM was used in this work, as shown in Figure 26. The device enables material imaging in micro and nano dimensions. In addition, the element content and distribution of the structures can be obtained with the EDX (energy dispersive x-ray spectroscopy) detector tied to the SEM.

Figure 26. FEI-SEM device

CHAPTER 4

RESULT AND DISCUSSION

The results of surface roughness, cutting force, wear, and chip form examination are reported and discussed to evaluate the machinability performance of the specimens in this chapter.

4.1. Surface Roughness Results

This section presents the measured surface roughness results analyzed through S/N ratio, ANOVA and regression methods.

4.1.1. Analysis of S/N ratio

Table 8 represents the surface roughness results and calculated S/N ratios of them based on the "smaller is better" (eq. 3.1) approach. The table shows that the optimum machinability condition was obtained in experiment 3 as it displays minimum Ra with maximum S/N ratio.

Table 8. Measured surface roughness and calculated S/N ratio values

Exp. No.	Material	V_c (m/min)	V_f (mm/min)	Ra (µm)	S/N ratio (dB)
1	AZ91	480	0.65	0.524 ± 0.03	5.613
2	AZ91	560	0.80	0.427 ± 0.05	7.391
3	AZ91	640	0.95	0.384 ± 0.01	8.313
4	AZ91/2.5 wt.% rCF	480	0.80	0.798 ± 0.17	1.959
5	AZ91/2.5 wt.% rCF	560	0.95	0.555 ± 0.16	5.114
6	AZ91/2.5 wt.% rCF	640	0.65	0.477 ± 0.02	6.429
7	AZ91/5 wt.% rCF	480	0.95	0.957 ± 0.39	0.381
8	AZ91/5 wt.% rCF	560	0.65	0.518 ± 0.32	5.713
9	AZ91/5 wt.% rCF	640	0.80	0.794 ± 0.15	2.003

Table 9 shows the surface roughness response table for the S/N ratios. Figure 27 represents the plotted response data. The response table reveals that the material is the most influential factor on the surface roughness, and the least influential factor is the feed rate, based on their rank. As seen in Figure 27, the optimal parameters are as follows: the material of AZ91, the cutting speed of 560 m/min and the feed rate of 0.65 mm/min. The S/N ratios demonstrated that higher cutting speeds and lower feed rates led to lower surface roughness results while increasing reinforcement content increased the surface roughness.

Table 9. Surface roughness response table for S/N ratios

Level	Material	Cutting Speed (m/min)	Feed Rate (mm/min)
1	7.106	2.652	5.919
2	4.501	6.073	3.785
3	2.700	5.582	4.603
Delta	4.406	3.421	2.134
Rank	1	2	3

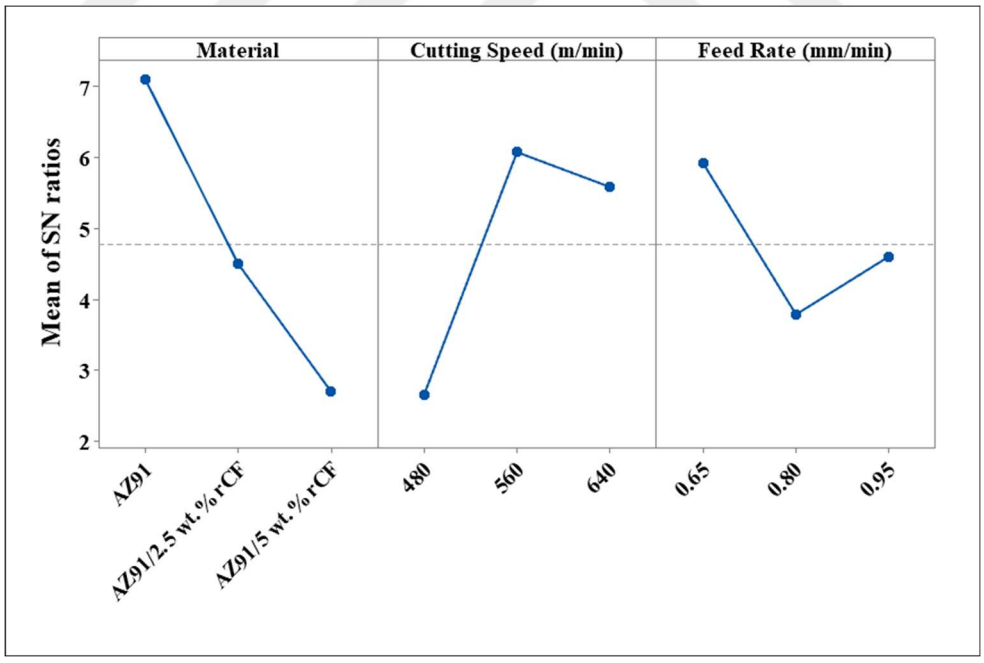

Figure 27. Main effect plots for S/N ratios of surface roughness

4.1.2. Analysis of Variance (ANOVA)

ANOVA results calculated for the surface roughness at a 95% confidence interval are presented in Table 10.

Table 10. ANOVA results for surface roughness

Factor	DF	Seq SS	Adj MS	P-value	Contribution
Material	2	0.145	0.072	0.041	46.90%
V_c (m/min)	2	0.113	0.056	0.052	36.52%
V_f (mm/min)	2	0.045	0.022	0.121	14.58%
Error	2	0.006	0.003	-	2.00%
Total	8	0.310	-	-	100.00%
R-sq: 98%					

According to the ANOVA results, the material factor exhibited statistical significance with a p-value of 0.041 on the surface roughness. The material factor affected the surface roughness at a rate of 46.90%. The cutting speed and feed rate have less effect on the surface roughness at 36.52% and 14.58%, respectively. The error rate of 2.00% can be attributed to factors not considered in the experimental study, such as machine vibration, cutting tool properties, material defects, etc.

The effects of material and cutting speed factors on the surface roughness are shown in Figure 28. According to the figure, the surface roughness of AZ91 alloy slightly decreases as the cutting speed increases. It was observed that an increase in the cutting speed led to a remarkable change in both composites. While increasing cutting speed continuously decreases the surface roughness of 2.5 wt.% rCF reinforced composite, that of 5 wt.% rCF reinforced composite fluctuated.

Figure 29 depicts the effects of material and feed rate factors on the surface roughness. The feed rate did not show a considerable effect for AZ91 alloy, excluding a slight decrease. The feed rate demonstrated a remarkable trend over the composites. Both composites provided lower surface roughness values at lower feed rates. An increase in the feed rate generally led to increased surface roughness for the composites. The surface roughness of 2.5 wt.% rCF reinforced composite fluctuated at feed rates around 0.95 mm/min.

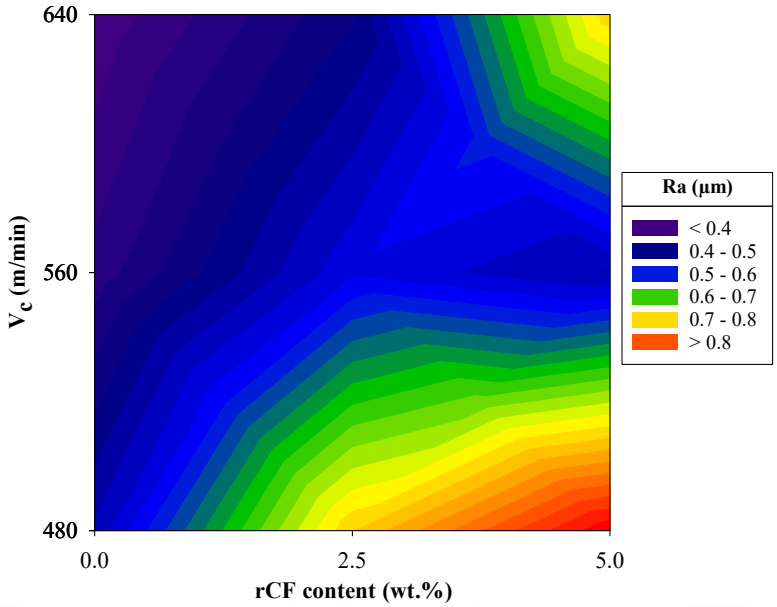

Figure 28. Contour plot for surface roughness vs. rCF content and cutting speed

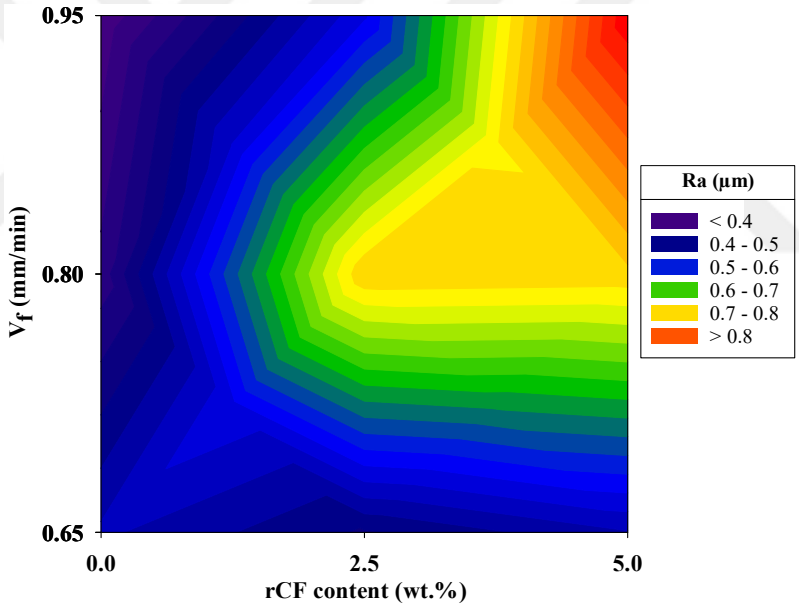

Figure 29. Contour plot for surface roughness vs. rCF content and feed rate

The results revealed that the most promising surface roughness performance was obtained for AZ91 alloy, while the poorest performance was obtained for 5 wt.% rCF reinforced composite. This outcome shows that the increasing reinforcement content increases the surface roughness. This result is consistent with the studies of Jadhav et al.[86], and Ozben et al.[87] As reported by Jadhav et al., Al_2O_3 reinforcement (10 wt.%) increased the surface roughness in the machining of Al6061 and its composite. Ozben et

al. stated that higher surface roughness values were measured as the reinforcement content increased in the machining of $AlSi_7Mg_2$/SiC (2, 4 and 6 wt.%) MMCs.

4.1.3. Analysis of Regression

Regression analysis was used to derive the equations for the surface roughness output. The equations were developed as linear and quadratic models at a 95% confidence interval. The equations 4.1-4.3 represent the linear model, and 4.4-4.6 represent the quadratic model. The calculated R-sq values are 75.44% and 98.39% for the linear and quadratic models. Since the quadratic regression model has a higher R-sq value, it was used to estimate the surface roughness. Figure 30 compares the experimental results and predicted values calculated via the quadratic model. The figure shows that the values are relatively close to the regression line. The values are within the confidence interval (CI), and there is no value outside the prediction interval (PI). A relatively high correlation was obtained between the results.

$$AZ91 = 0.838 - 0.001300\,V_c + 0.419\,V_f \tag{4.1}$$

$$AZ91/2.5\,wt.\%\,rCF = 1.003 - 0.001300\,V_c + 0.419\,V_f \tag{4.2}$$

$$AZ91/5\,wt.\%\,rCF = 1.149 - 0.001300\,V_c + 0.419\,V_f \tag{4.3}$$

$$\begin{aligned} AZ91 = {} & 4.57 - 0.02689\,V_c + 8.96\,V_f + 0.000024\,{V_c}^2 \\ & -4.61{V_f}^2 - 0.00207\,V_cV_f \end{aligned} \tag{4.4}$$

$$\begin{aligned} AZ91/2.5\,wt.\%\,rCF = {} & 4.71 - 0.02689\,V_c + 8.96\,V_f + 0.000024\,{V_c}^2 \\ & -4.61{V_f}^2 - 0.00207\,V_cV_f \end{aligned} \tag{4.5}$$

$$\begin{aligned} AZ91/5\,wt.\%\,rCF = {} & 4.85 - 0.02689\,V_c + 8.96\,V_f + 0.000024\,{V_c}^2 \\ & -4.61{V_f}^2 - 0.00207\,V_cV_f \end{aligned} \tag{4.6}$$

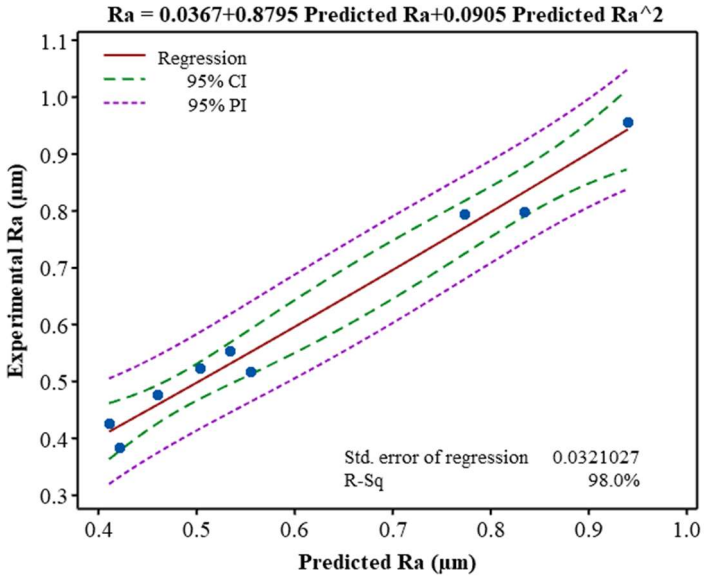

Figure 30. Comparison of experimental and predicted values for surface roughness

4.2. Cutting Force Results

The measured cutting forces analyzed through S/N ratio, ANOVA and regression methods were provided in this section.

4.2.1. Analysis of S/N Ratio

The cutting forces and calculated S/N ratios of them based on the "smaller is better" approach are shown in Table 11. The table shows that the optimum machinability condition was obtained in experiment 6 as it displays minimum average cutting force with maximum S/N ratio.

The cutting force response table for the S/N ratios is shown in Table 12. Figure 31 depicts the plotted response data. The response table reveals that the material is the most influential factor in the cutting force, and the cutting speed has the lowest effect, based on their rank. As demonstrated in Figure 31, the optimal machinability performance for the cutting force output can be achieved in machining AZ91 alloy at the cutting speed of 640 m/min and the feed rate of 0.65 mm/min. The S/N ratio results showed that the increasing reinforcement content increased the cutting forces. In addition, higher cutting speeds and lower feed rates provided the most promising cutting force results.

Table 11. Measured cutting force and calculated S/N ratio values

Exp. No.	Material	V_c (m/min)	V_f (mm/min)	F_c (N)	S/N ratio (dB)
1	AZ91	480	0.65	38.212 ± 4.69	-31.644
2	AZ91	560	0.80	30.198 ± 4.44	-29.599
3	AZ91	640	0.95	39.539 ± 6.84	-31.940
4	AZ91/2.5 wt.% rCF	480	0.80	40.454 ± 1.36	-32.139
5	AZ91/2.5 wt.% rCF	560	0.95	51.316 ± 1.34	-34.205
6	AZ91/2.5 wt.% rCF	640	0.65	26.309 ± 3.10	-28.402
7	AZ91/5 wt.% rCF	480	0.95	72.452 ± 15.67	-37.201
8	AZ91/5 wt.% rCF	560	0.65	55.557 ± 3.33	-34.894
9	AZ91/5 wt.% rCF	640	0.80	58.535 ± 3.12	-35.348

Table 12. Cutting force response table for S/N ratios

Level	Material	Cutting Speed (m/min)	Feed Rate (mm/min)
1	-31.06	-33.66	-31.65
2	-31.58	-32.90	-32.36
3	-35.81	-31.90	-34.45
Delta	4.75	1.76	2.80
Rank	1	3	2

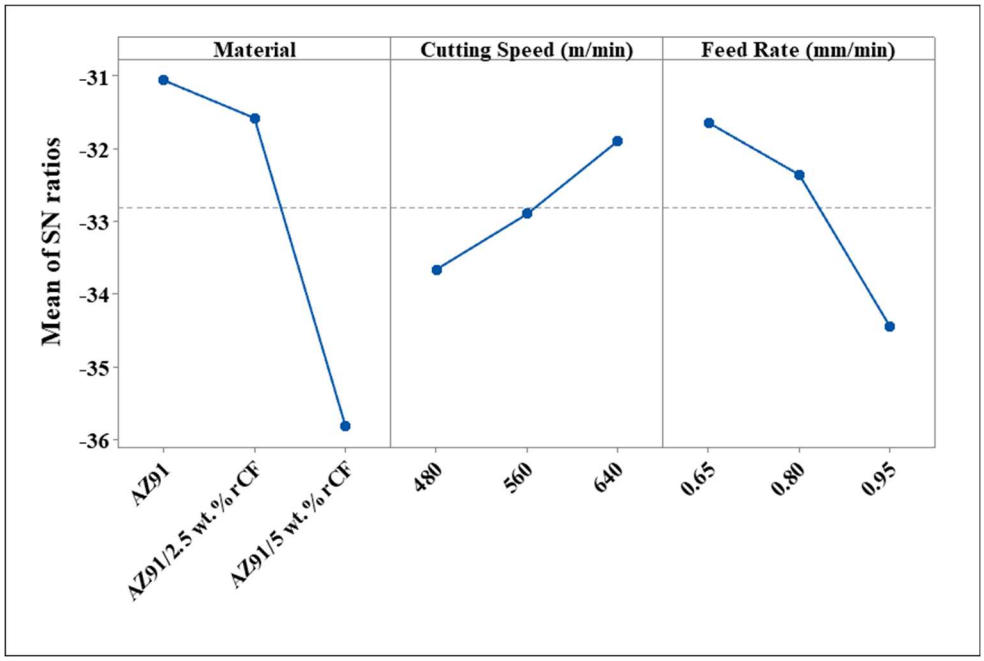

Figure 31. Main effect plots for S/N ratios of cutting force

4.2.2. Analysis of Variance (ANOVA)

Table 13 provides ANOVA results calculated for the cutting force at a 95% confidence interval.

Table 13. ANOVA results for cutting force

Factor	DF	Seq SS	Adj MS	P-Value	Contribution
Material	2	1218.58	609.29	0.049	69.76%
V_c (m/min)	2	119.23	59.61	0.345	6.83%
V_f (mm/min)	2	346.21	173.11	0.153	19.82%
Error	2	62.78	31.39	-	3.59%
Total	8	1746.80	-	-	100.00%
R-sq: 96.41%					

The ANOVA results reveal that the material factor is statistically significant, with a p-value of 0.049 on the cutting force. The material is the most influential factor at a rate of 69.76%. The feed rate and cutting speed affected the cutting force at 19.82% and 6.83% contribution rates, respectively. The error rate of 3.59% can be attributed to the factors not considered in the study.

Figure 32 depicts the influences of material and cutting speed factors on the cutting force. According to the figure, the cutting speed did not significantly affect the cutting force for AZ91 alloy. In addition, the cutting speed did not show a relatively notable effect in machining 2.5 wt.% rCF reinforced composite except for fluctuations at moderate cutting speeds. The cutting speed demonstrated a remarkable effect for 5 wt.% rCF reinforced composite, and higher cutting forces were observed for this composite at lower cutting speeds.

The effects of material and feed rate factors on the cutting force are shown in Figure 33. The figure reveals that the feed rate has no considerable influence on the AZ91 alloy. Higher cutting forces were observed at higher feed rates in the machining 2.5 wt.% rCF composite. The feed rate exhibited a significant effect on the 5 wt.% rCF reinforced composite, and the cutting forces continuously increased as the feed rate increased.

The results demonstrated that the most desirable cutting force performance was acquired for AZ91 alloy, while the most unsatisfactory performance was acquired for 5 wt.% rCF reinforced composite. This outcome shows that the increasing reinforcement

content increases the cutting force. As reported in the study of Jiang et al.[88], higher cutting forces were measured in the machining of Al7050/TiB_2 (titanium diboride) (6 vol.%) MMC compared to Al7050 alloy. Juliyana and Prakash[89] examined the machinability of LM5/ZrO_2 (zirconia) (3,6 and 9 wt.%) MMCs. The study revealed that increasing ZrO_2 content increased the thrust force.

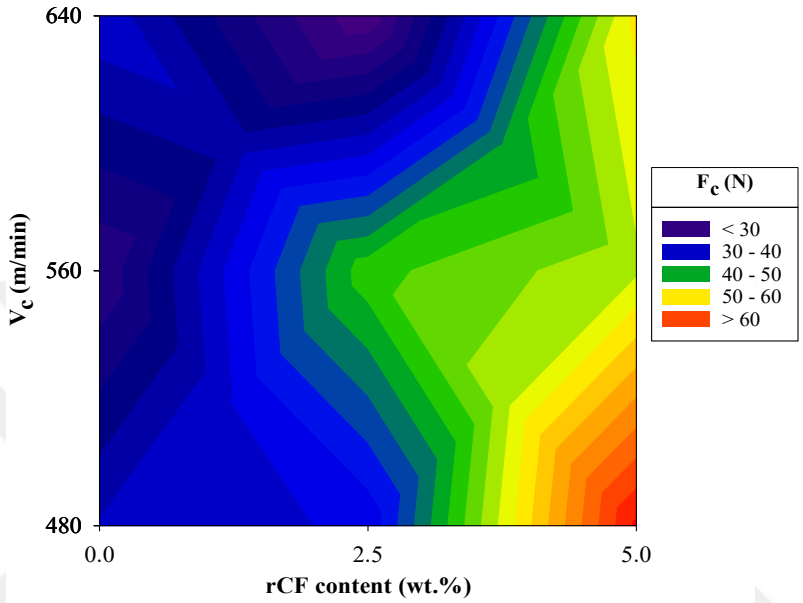

Figure 32. Contour plot for cutting force vs. rCF content and cutting speed

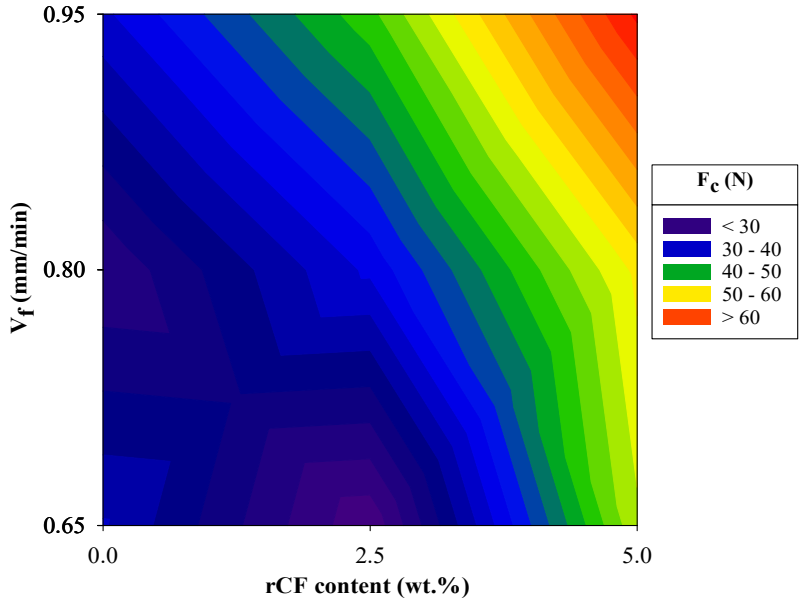

Figure 33. Contour plot for cutting force vs. rCF content and feed rate

4.2.3. Analysis of Regression

The regression equations were derived for the cutting force output at a 95% confidence interval. The linear model includes the equations 4.7-4.9, and the quadratic model includes the equations 4.10-4.12. The R-sq values are 94.41% and 98.51% for the linear and quadratic models. Both models can successfully estimate the cutting force based on their relatively high R-sq values. The quadratic model was considered for the cutting force output as it displays a higher R-sq value. Figure 34 compares the experimental results and predicted values calculated via the quadratic model. The values are relatively close to the regression line. A relatively high correlation was obtained between the experimental results and predicted values.

$$AZ91 = 28.7 - 0.0557\,V_c + 48\,V_f \tag{4.7}$$

$$AZ91/2.5\,wt.\%\,rCF = 32.1 - 0.0557\,V_c + 48\,V_f \tag{4.8}$$

$$AZ91/5\,wt.\%\,rCF = 54.9 - 0.0557\,V_c + 48\,V_f \tag{4.9}$$

$$AZ91 = 313 - 0.381\,V_c - 448\,V_f + 0.000035\,{V_c}^2 + 185\,{V_f}^2 + 0.357\,V_cV_f \tag{4.10}$$

$$AZ91/2.5\,wt.\%\,rCF = 320 - 0.381\,V_c - 448\,V_f + 0.000035\,{V_c}^2 + 185\,{V_f}^2 + 0.357\,V_cV_f \tag{4.11}$$

$$AZ91/5\,wt.\%\,rCF = 343 - 0.381\,V_c - 448\,V_f + 0.000035\,{V_c}^2 + 185\,{V_f}^2 + 0.357\,V_cV_f \tag{4.12}$$

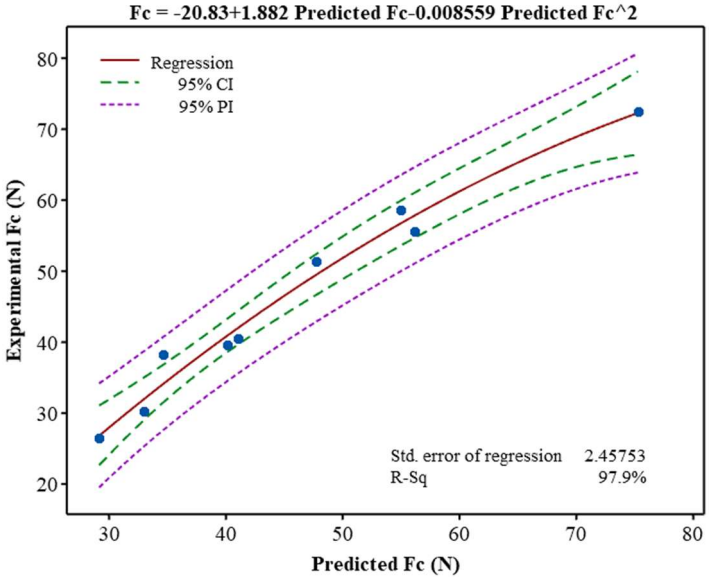

Figure 34. Comparison of experimental and predicted values for cutting force

4.3. Material Characterization

The results of employed characterization methods are reported and discussed in the following sections.

4.3.1. SEM Results

Figure 35 presents the SEM micrographs of the specimens. The figure reveals that the rCFs were uniformly distributed vertically and horizontally into the matrix without any preferential orientation into the alloy. This indicates that the HSD method can be an effective alternative to distribute the reinforcements. In addition, Kandemir et al.[67] reported a few clusters of the rCFs for the AZ91/5 wt.% rCF composite.

Figure 36 shows the SEM images of the cutting inserts after the machining process. The SEM results are numbered as " experiment number.insert number ". From the SEM analysis of the cutting inserts, dominant BUL formations were observed on the rake surfaces of the inserts. Relatively denser layers were generated at 0.95 mm/min feed rates, and higher cutting forces were measured in these experiments. This can be assigned to the increasing cutting temperatures due to higher cutting forces, which make the workpiece material adhere more easily. In addition to BUL formation, some chips adhered to the inserts in experiment 3, as demonstrated in Figure 37. This can be ascribed to the selected cutting parameters with the highest speed and feed rate raising temperature.

In addition, non-notable BUE formations were seen on the cutting edge of inserts in experiments 6 and 8, as seen in Figure 38. In addition, Parra et al.[53] investigated the BUL and BUE formations in the machining of Al2024 and Al7050 alloys, and they reported that the formations of BUL and BUE are highly dependent on the temperature and can be observed at a wide range of cutting temperatures. Also, considering that the experiments were performed under dry cutting conditions, using a lubricant or coolant can be suggested to reduce the formation of BUL for this study.

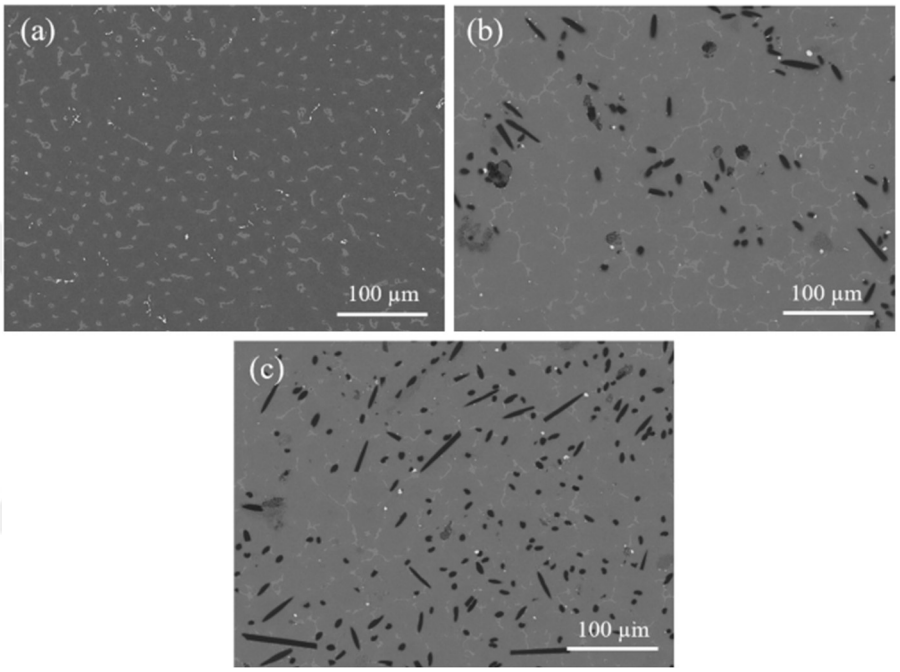

Figure 35. SEM images of a) AZ91 alloy, b) AZ91/2.5 wt.% rCF, c) AZ91/5 wt.% rCF

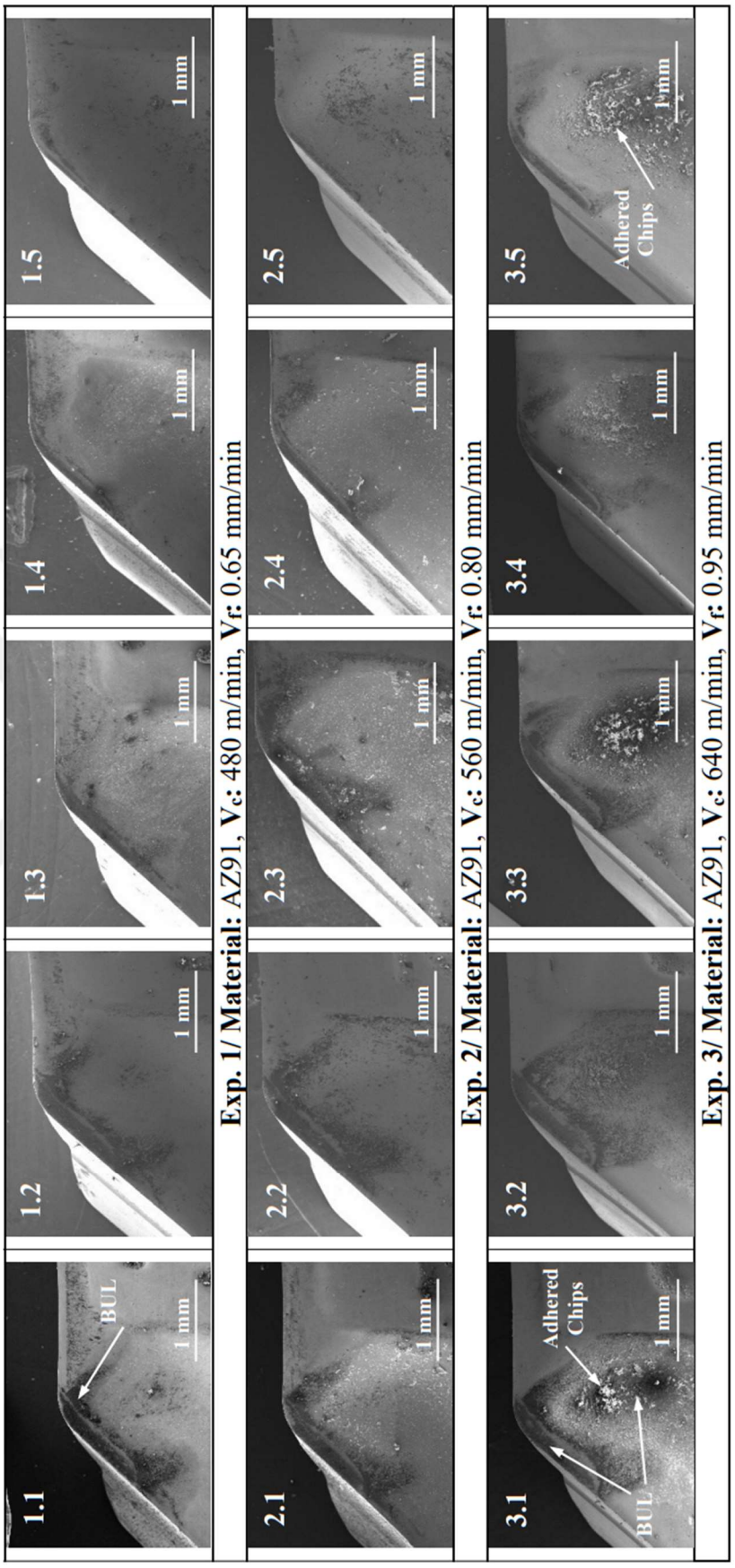

(Cont. on next page)

Figure 36. SEM images of cutting inserts

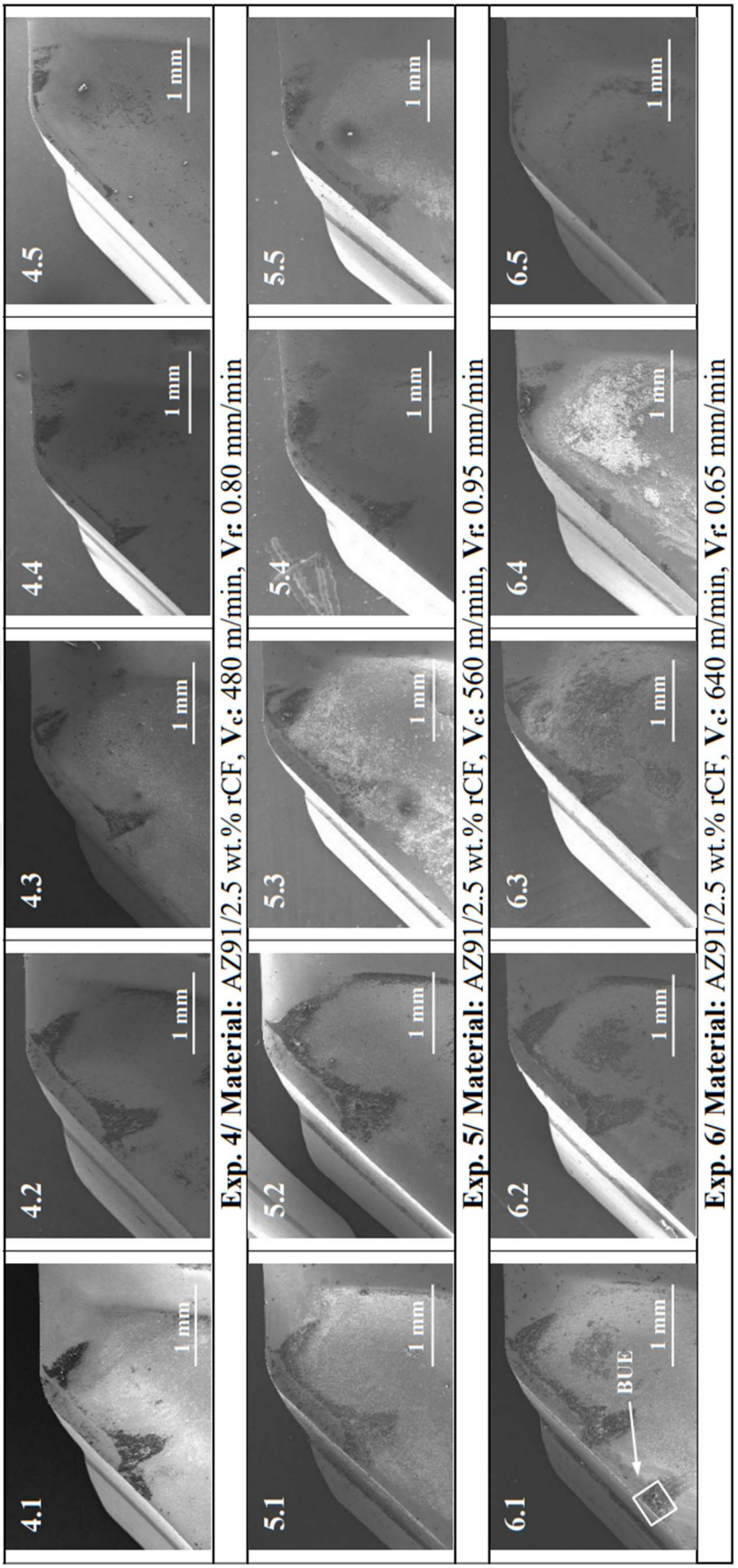

(Cont. on next page)

Figure 36. **(cont.)**

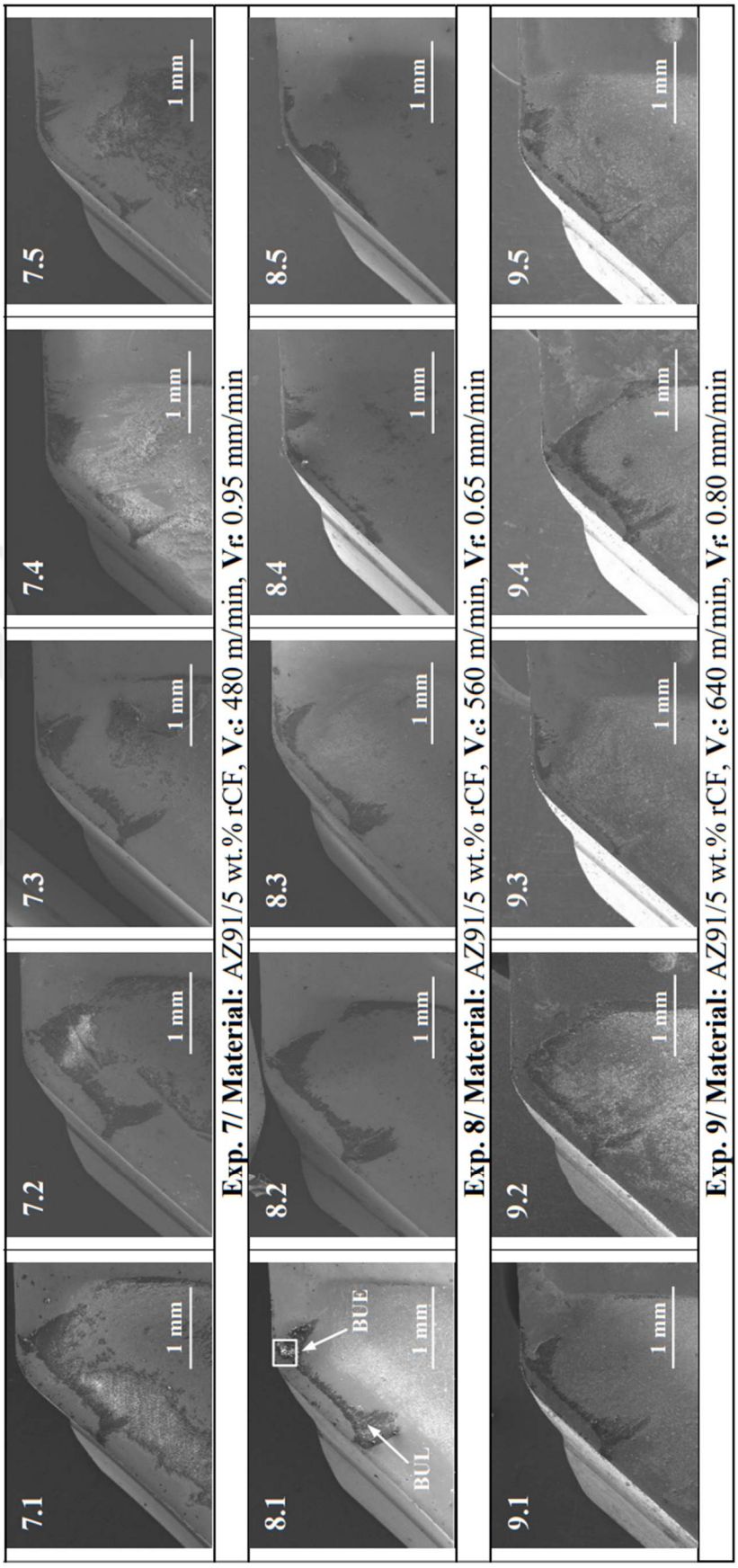

Figure 36. **(cont.)**

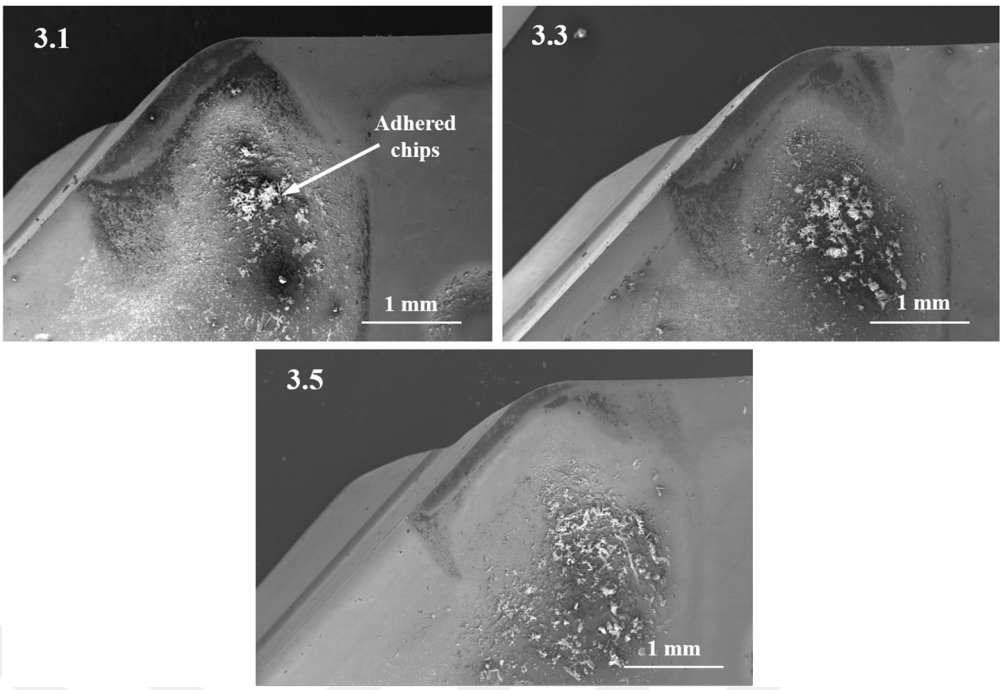

Figure 37. Adhered chip formations in experiment 3

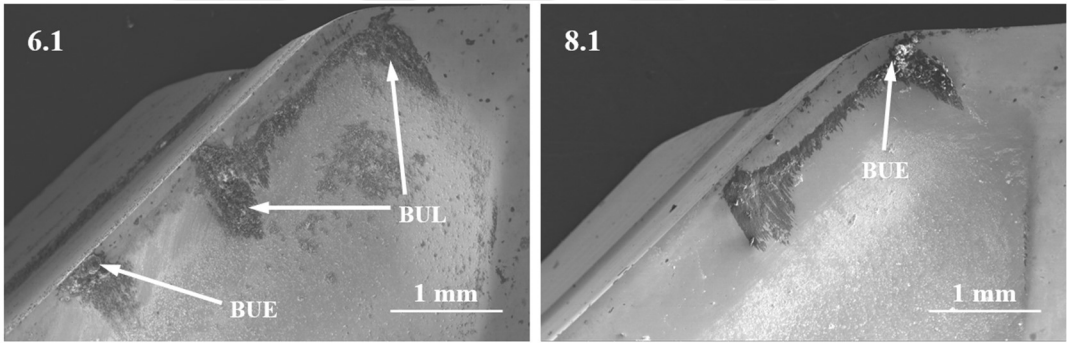

Figure 38. BUE formations in experiments 6 and 8

4.3.2. EDX Results

The EDX analysis was subjected to the selected regions of the insert 1 in experiment 1, as shown in Figure 39. As a result of the analysis, Mg and Al (the main elements of the matrix) were detected in the selected regions. In addition, W from the insert was not detected in some regions (spectrums 1 and 4), indicating that dense layers were generated in these regions.

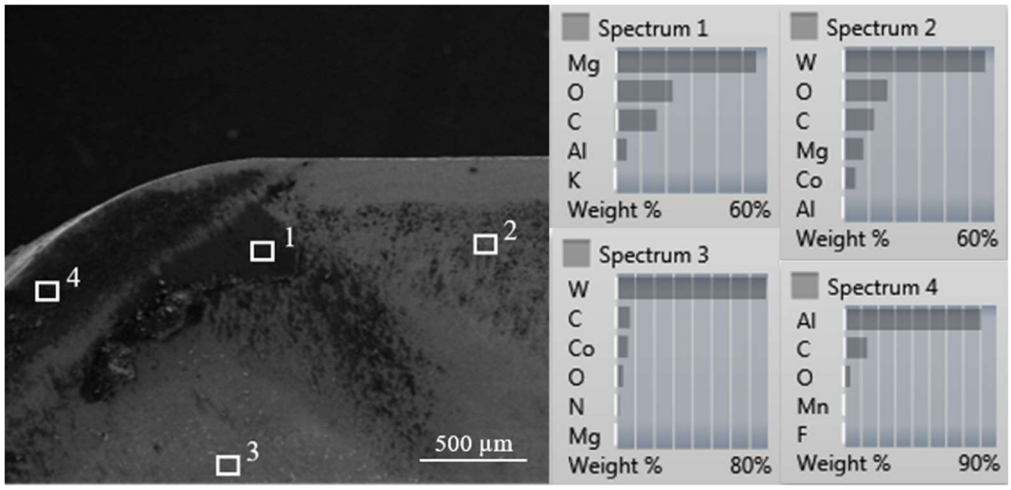

Figure 39. EDX analysis results of selected regions

4.4. Chip Form Analysis

Spiral shaped continuous chips were dominantly observed in the study, as shown in Figures 40-48. In addition to continuous chips, discontinuous chips were seen where the feed rate was relatively higher. Moreover, the chips shortened, and the discontinuous chip formation increased as the reinforcement content increased. This can be ascribed to increased brittleness. Sap et al.[90] also reported a similar result in machining of Cu (copper)/Ti-B (boron)-SiC (0-2-4-6-8 wt.%) MMCs. It has been reported that the chips got smaller as the feed rate and Ti-B-SiC content increased.

Figure 40. Chip forms of AZ91 alloy at conditions: V_c:480 m/min, V_f:0.65 mm/min

Figure 41. Chip forms of AZ91 alloy at conditions: V_c:560 m/min, V_f:0.80 mm/min

Figure 42. Chip forms of AZ91 alloy at conditions: V_c:640 m/min, V_f:0.95 mm/min

Figure 43. Chip forms of AZ91/2.5 wt.% rCF composite at conditions: V_c:480 m/min, V_f:0.80 mm/min

Figure 44. Chip forms of AZ91/2.5 wt.% rCF composite at conditions: V_c:560 m/min, V_f:0.95 mm/min

Figure 45. Chip forms of AZ91/2.5 wt.% rCF composite at conditions: V_c:640 m/min, V_f:0.65 mm/min

Figure 46. Chip forms of AZ91/5 wt.% rCF composite at conditions: V_c:480 m/min, V_f:0.95 mm/min

Figure 47. Chip forms of AZ91/5 wt.% rCF composite at conditions: V_c:560 m/min, V_f:0.65 mm/min

Figure 48. Chip forms of AZ91/5 wt.% rCF composite at conditions: V_c:640 m/min, V_f:0.80 mm/min

CHAPTER 5

CONCLUSIONS

In this study, the machinability of rCF reinforced Mg matrix composites was investigated. AZ91 alloy and its composites containing 2.5 and 5 wt.% rCF were conducted to the face milling operation at different cutting parameters. Surface roughness, cutting forces, wear on the cutting inserts and chip forms were examined to evaluate the machinability performance of the specimens.

The most favorable surface roughness performance was obtained for AZ91 alloy, while the most unsatisfactory performance was achieved for 5 wt.% rCF reinforced composite. The rCF content was the most effective parameter on the surface roughness at 46.90%. The increasing rCF content led to an increase in the surface roughness. The cutting speed and feed rate parameters influenced the surface roughness at 36.52% and 14.58%, respectively. The cutting speed and feed rate factors did not exhibit a noticeable effect for AZ91 alloy. Higher cutting speeds and lower feed rates generally decreased the surface roughness of the composites except for the fluctuations at certain points.

AZ91 alloy demonstrated the most satisfactory cutting force performance, while 5 wt.% rCF reinforced composite displayed the most undesirable performance. The rCF content was the most effective factor on the cutting force at 69.76%, and the increasing rCF content increased the cutting forces. The cutting speed and feed rate affected the cutting force at 6.83% and 19.82%, respectively. The cutting parameters did not reveal a remarkable change for AZ91 alloy. Lower cutting forces were generally measured at higher cutting speeds and lower feed rates in the machining of the composites.

As a result of the SEM and EDX analyses, considerable BUL formations were observed on the rake faces of the cutting inserts for each experiment. Relatively denser layers were formed at higher feed rates and were attributed to the increasing cutting temperature.

In the study, spiral shaped continuous chips were generally generated. Discontinuous chips were obtained in addition to the continuous chips at higher feed rates. The increasing reinforcement content resulted in the shortening of the chips and increased discontinuous chip formation attributed to the increased brittleness.

Overall, the findings of this study show that the rCF reinforced Mg matrix composites are machinable, and the selected cutting parameters are suitable for potential engineering applications. Considering the limited number of studies on carbon fiber reinforced Mg matrix composites, future study is recommended to evaluate the full machinability potential of such composites for engineering applications. Future studies can include modification of the cutting parameters, influence of cutting insert properties and reduction of the BUL formation.

REFERENCES

(1) Zhang, B.; Hou, Y.; Wang, X.; Wang, Y.; Geng, L. Mechanical Properties, Degradation Performance and Cytotoxicity of Mg–Zn–Ca Biomedical Alloys with Different Compositions. *Materials Science and Engineering: C* **2011**, *31* (8), 1667–1673. https://doi.org/10.1016/J.MSEC.2011.07.015.

(2) Gupta, M.; Sharon, N. M. L. *Magnesium, Magnesium Alloys, and Magnesium Composites*; WILEY, **2010**. https://doi.org/10.1002/9780470905098.

(3) Fujisawa, S.; Yonezu, A. Mechanical Property of Microstructure in Die-Cast Magnesium Alloy Evaluated by Indentation Testing at Elevated Temperature. In *Recent Advances in Structural Integrity Analysis - Proceedings of the International Congress (APCF/SIF-2014)*; Elsevier, **2014**; pp 422–426. https://doi.org/10.1533/9780081002254.422.

(4) Bledzki, A. K.; Seidlitz, H.; Goracy, K.; Urbaniak, M.; Rösch, J. J. Recycling of Carbon Fiber Reinforced Composite Polymers-Review-Part 1: Volume of Production, Recycling Technologies, Legislative Aspects. *Polymers*. **2021**, pp 1–13. https://doi.org/10.3390/polym13020300.

(5) Nagavally, R. R. Composite Materials - History, Types, Fabrication Techniques, Advantages, and Applications. *International Journal of Mechanical And Production Engineering* **2016**, 25–30.

(6) Sajan, S.; Philip Selvaraj, D. A Review on Polymer Matrix Composite Materials and Their Applications. *Mater Today Proc* **2021**, *47*, 5493–5498. https://doi.org/10.1016/J.MATPR.2021.08.034.

(7) Chawla, K. K. *Composite Materials: Science and Engineering*; **2019**. https://doi.org/10.1007/978-3-030-28983-6.

(8) Clyne, T. W.; Hull, D. *An Introduction to Composite Materials*; **2019**. https://doi.org/10.1017/9781139050586.

(9) Meignanamoorthy, M.; Ravichandran, M.; Alagarsamy, S. V.; Chanakyan, C.; Kumar, S. D.; Sakthivelu, S. Effect of Various Reinforcements on Properties of Metal Matrix Composites: A Review. *Mater Today Proc* **2020**, *27*, 1118–1121. https://doi.org/10.1016/J.MATPR.2020.01.479.

(10) Bahl, S. Fiber Reinforced Metal Matrix Composites - a Review. *Mater Today Proc* **2021**, *39*, 317–323. https://doi.org/10.1016/J.MATPR.2020.07.423.

(11) Moncy, A.; Castro, O.; Berggreen, C.; Stang, H. Understanding the Effect of Anisotropy in Composite Materials on the Performance of Cruciform Specimens. *Compos Struct* **2021**, *273*, 1–12. https://doi.org/10.1016/J.COMPSTRUCT.2021.114225.

(12) Shirvanimoghaddam, K.; Hamim, S. U.; Karbalaei Akbari, M.; Fakhrhoseini, S. M.; Khayyam, H.; Pakseresht, A. H.; Ghasali, E.; Zabet, M.; Munir, K. S.; Jia, S.; Davim, J. P.; Naebe, M. Carbon Fiber Reinforced Metal Matrix Composites: Fabrication Processes and Properties. *Compos Part A Appl Sci Manuf* **2017**, *92*, 70–96. https://doi.org/10.1016/J.COMPOSITESA.2016.10.032.

(13) Holmes, M. Recycled Carbon Fiber Composites Become a Reality. *Reinforced Plastics* **2018**, *62* (3), 148–153. https://doi.org/10.1016/j.repl.2017.11.012.

(14) Akonda, M. H.; Lawrence, C. A.; Weager, B. M. Recycled Carbon Fibre-Reinforced Polypropylene Thermoplastic Composites. *Compos Part A Appl Sci Manuf* **2012**, *43* (1), 79–86. https://doi.org/10.1016/j.compositesa.2011.09.014.

(15) Meng, F.; McKechnie, J.; Turner, T.; Wong, K. H.; Pickering, S. J. Environmental Aspects of Use of Recycled Carbon Fiber Composites in Automotive Applications. *Environ Sci Technol* **2017**, *51* (21), 12727–12736. https://doi.org/10.1021/acs.est.7b04069.

(16) Witik, R. A.; Teuscher, R.; Michaud, V.; Ludwig, C.; Månson, J. A. E. Carbon Fibre Reinforced Composite Waste: An Environmental Assessment of Recycling, Energy Recovery and Landfilling. *Compos Part A Appl Sci Manuf* **2013**, *49*, 89–99. https://doi.org/10.1016/j.compositesa.2013.02.009.

(17) Bledzki, A. K.; Seidlitz, H.; Krenz, J.; Goracy, K.; Urbaniak, M.; Rösch, J. J. Recycling of Carbon Fiber Reinforced Composite Polymers—Review—Part 2: Recovery and Application of Recycled Carbon Fibers. *Polymers*. **2020**. https://doi.org/10.3390/polym12123003.

(18) Oladijo, O. P.; Awe, S. A.; Akinlabi, E. T.; Phiri, R. R.; Collieus, L. L.; Phuti, R. E. High-Temperature Properties of Metal Matrix Composites. In *Encyclopedia of Materials: Composites*; Brabazon, D., Ed.; Elsevier, **2021**; Vol. 1, pp 360–374. https://doi.org/10.1016/B978-0-12-819724-0.00096-3.

(19) Kaczmar, J. W.; Pietrzak, K.; Wlosiński, W. Production and Application of Metal Matrix Composite Materials. *J Mater Process Technol* **2000**, *106* (1–3), 58–67. https://doi.org/10.1016/S0924-0136(00)00639-7.

(20) Sharma, D. K.; Mahant, D.; Upadhyay, G. Manufacturing of Metal Matrix Composites: A State of Review. In *Materials Today: Proceedings*; **2019**; Vol. 26, pp 506–519. https://doi.org/10.1016/j.matpr.2019.12.128.

(21) Kumar, A.; Kumar, S.; Mukhopadhyay, N. K. Introduction to Magnesium Alloy Processing Technology and Development of Low-Cost Stir Casting Process for Magnesium Alloy and Its Composites. *Journal of Magnesium and Alloys* **2018**, *6* (3), 245–254. https://doi.org/10.1016/j.jma.2018.05.006.

(22) Ramanathan, A.; Krishnan, P. K.; Muraliraja, R. A Review on the Production of Metal Matrix Composites through Stir Casting – Furnace Design, Properties, Challenges, and Research Opportunities. *J Manuf Process* **2019**, *42*, 213–245. https://doi.org/10.1016/j.jmapro.2019.04.017.

(23) Sajjadi, S. A.; Ezatpour, H. R.; Beygi, H. Microstructure and Mechanical Properties of Al-Al2O3 Micro and Nano Composites Fabricated by Stir Casting. *Materials Science and Engineering A* **2011**, *528* (29–30), 8765–8771. https://doi.org/10.1016/j.msea.2011.08.052.

(24) Seetharaman, S.; Subramanian, J.; Singh, R. A.; Wong, W. L. E.; Nai, M. L. S.; Gupta, M. Mechanical Properties of Sustainable Metal Matrix Composites: A Review on the Role of Green Reinforcements and Processing Methods. *Technologies*. February 16, **2022**, pp 1–27. https://doi.org/10.3390/technologies10010032.

(25) Seetharaman, S.; Gupta, M. *Fundamentals of Metal Matrix Composites*; **2021**; Vol. 1. https://doi.org/10.1016/B978-0-12-819724-0.00001-X.

(26) Rajendran, S. H.; Cho, D. H.; Jung, J. P. Comparative Study on the Wettability and Thermal Aging Characteristics of SAC 305 Nanocomposite Solder Fabricated by Stir-Casting and Ultrasonic Treatment. *Mater Today Commun* **2022**, *31*, 1–15. https://doi.org/10.1016/j.mtcomm.2022.103814.

(27) Kondoh, K.; Kawakami, M.; Imai, H.; Umeda, J.; Fujii, H. Wettability of Pure Ti by Molten Pure Mg Droplets. *Acta Mater* **2010**, *58* (2), 606–614. https://doi.org/10.1016/j.actamat.2009.09.039.

(28) Malaki, M.; Tehrani, A. F.; Niroumand, B.; Gupta, M. Wettability in Metal Matrix Composites. *Metals*. June 28, **2021**, pp 1–24. https://doi.org/10.3390/met11071034.

(29) Huhtamäki, T.; Tian, X.; Korhonen, J. T.; Ras, R. H. A. Surface-Wetting Characterization Using Contact-Angle Measurements. *Nat Protoc* **2018**, *13* (7), 1521–1538. https://doi.org/10.1038/s41596-018-0003-z.

(30) Davim, J. P. *Machining: Fundamentals and Recent Advances*; **2008**. https://doi.org/10.1007/978-1-84800-213-5.

(31) Knight, W. A.; Boothroyd, G. *Fundamentals of Metal Machining and Machine Tools*; **2019**. https://doi.org/10.1201/9780429114243.

(32) 'Xia, S. *What Differs Both Cutting Speed and Feed Rate in CNC Machining?*. BaiChuan. https://bccncmilling.com/what-differs-both-cutting-speed-and-feed-rate-in-cnc-machining/ (accessed 2023-05-03).

(33) Zheng, H.; Liu, K. Machinability of Engineering Materials. In *HandBook of Manufacturing Engineering and Technology*; **2014**; pp 1–34. https://doi.org/10.1007/978-1-4471-4670-4_2.

(34) David, C.; Sagris, D.; Stergianni, E.; Tsiafis, C.; Tsiafis, I. Experimental Analysis of the Effect of Vibration Phenomena on Workpiece Topomorphy Due to Cutter Runout in End-Milling Process. *Machines* **2018**, *6* (3), 1–11. https://doi.org/10.3390/machines6030027.

(35) Elmagrabi, N. H.; Shuaeib, F. M.; Haron, C. H. C. An Overview on the Cutting Tool Factors in Machinability Assessment. *Journal of Achievements in Materials and Manufacturing Engineering* **2007**, *23* (2), 2–5.

(36) Yılmaz, B.; Karabulut, S.; Gullu, A. A Review of the Chip Breaking Methods for Continuous Chips in Turning. *J Manuf Process* **2020**, *49*, 50–69. https://doi.org/10.1016/j.jmapro.2019.10.026.

(37) Liu, R.; Eaton, E.; Yu, M.; Kuang, J. An Investigation of Side Flow during Chip Formation in Orthogonal Cutting. In *Procedia Manufacturing*; Elsevier B.V., **2017**; Vol. 10, pp 568–577. https://doi.org/10.1016/j.promfg.2017.07.053.

(38) Alagan, N. T. Textured Insert for Improved Heat Extraction in Combination with High-Pressure Cooling in Turning of Superalloys. Licentiate Thesis, University West, Trollhättan, **2017**. http://www.diva-portal.org/smash/record.jsf?pid=diva2%3A1147489&dswid=-5367 (accessed 2023-05-18).

(39) Groover, M. P. *Fundamentals of Modern Manufacturing 4th Edition*; **2012**.

(40) Yılmaz, B.; Karabulut, Ş.; Güllü, A. Performance Analysis of New External Chip Breaker for Efficient Machining of Inconel 718 and Optimization of the Cutting Parameters. *J Manuf Process* **2018**, *32*, 553–563. https://doi.org/10.1016/j.jmapro.2018.03.025.

(41) Cascón, I.; Sarasua, J. A.; Elkaseer, A. Tailored Chip Breaker Development for Polycrystalline Diamond Inserts: FEM-Based Design and Validation. *Applied Sciences (Switzerland)* **2019**, *9* (19), 1–12. https://doi.org/10.3390/app9194117.

(42) Belhadi, S.; Mabrouki, T.; Rigal, J. F.; Boulanouar, L. Experimental and Numerical Study of Chip Formation during Straight Turning of Hardened AISI 4340 Steel. *Proc Inst Mech Eng B J Eng Manuf* **2005**, *219* (7), 515–524. https://doi.org/10.1243/095440505X32445.

(43) Alauddin, M.; Choudhury, I. A.; El Baradie, M. A.; Hashmi, M. S. J. Plastics and Their Machining: A Review. *Journal of Materials Processing Tech.* **1995**, *54* (1–4), 40–46. https://doi.org/10.1016/0924-0136(95)01917-0.

(44) Karpuschewski, B.; Bryne, G.; Denkena, B.; Oliveira, J.; Vereschaka, A. *Springer Handbook of Mechanical Engineering*, 2nd ed.; **2021**. https://doi.org/https://doi.org/10.1007/978-3-030-47035-7.

(45) Hou, J.; Zhou, W.; Zhao, N. Methods for Prevention of Ignition during Machining of Magnesium Alloys. *Key Eng Mater* **2010**, *447–448*, 150–154. https://doi.org/10.4028/www.scientific.net/KEM.447-448.150.

(46) Shane, T. *How to Choose the Right Face Milling Cutter: A Guide*. MachineMFG. https://www.machinemfg.com/guide-for-selection-of-face-milling-cutter/#google_vignette (accessed 2023-04-02).

(47) *Milling Inserts to Complete Cutting Tool Needs*. Wodenco. https://www.wodenco.com/milling-inserts/ (accessed 2023-05-11).

(48) Hua, J.; Shivpuri, R. A Cobalt Diffusion Based Model for Predicting Crater Wear of Carbide Tools in Machining Titanium Alloys. *J Eng Mater Technol* **2005**, *127* (1), 136–144. https://doi.org/10.1115/1.1839192.

(49) Astakhov, V. P. The Assessment of Cutting Tool Wear. *Int J Mach Tools Manuf* **2004**, *44* (6), 637–647. https://doi.org/10.1016/j.ijmachtools.2003.11.006.

(50) Liu, Z. Q.; Ai, X.; Zhang, H.; Wang, Z. T.; Wan, Y. Wear Patterns and Mechanisms of Cutting Tools in High-Speed Face Milling. *J Mater Process Technol* **2002**, *129* (1–3), 222–226. https://doi.org/10.1016/S0924-0136(02)00605-2.

(51) Jawaid, A.; Sharif, S.; Koksal, S. Evaluation of Wear Mechanisms of Coated Carbide Tools When Face Milling Titanium Alloy. *J Mater Process Technol* **2000**, *99* (1–3), 266–274. https://doi.org/10.1016/S0924-0136(99)00438-0.

(52) Kaltenbrunner, T.; Krückl, H. P.; Schnalzger, G.; Klünsner, T.; Teppernegg, T.; Czettl, C.; Ecker, W. Differences in Evolution of Temperature, Plastic Deformation and Wear in Milling Tools When up-Milling and down-Milling Ti6Al4V. *J Manuf Process* **2022**, *77*, 75–86. https://doi.org/10.1016/j.jmapro.2022.03.010.

(53) Gómez-Parra, A.; Álvarez-Alcón, M.; Salguero, J.; Batista, M.; Marcos, M. Analysis of the Evolution of the Built-Up Edge and Built-Up Layer Formation Mechanisms in the Dry Turning of Aeronautical Aluminium Alloys. *Wear* **2013**, *302* (1–2), 1209–1218. https://doi.org/10.1016/j.wear.2012.12.001.

(54) Bjorn, H. *Cutting tool wear*. Manufacturing Guide. https://www.manufacturingguide.com/en/ordlista/cutting-tool-wear (accessed 2023-06-01).

(55) Gokkaya, H. The Effects of Machining Parameters on Cutting Forces, Surface Roughness, Built-up Edge (BUE) and Built-up Layer (BUL) during Machining AA2014 (T4) Alloy. *Journal of Mechanical Engineering* **2010**, *56* (9), 584–593.

(56) Surya, G.; Krishna, K.; Sameer, S.; Bhargavi, M.; Kumar, B.; Rao, G.; Naidubabu, Y.; Dumpala, R.; Sunil, B. Machining Characteristics of Fine Grained AZ91 Mg Alloy Processed by Friction Stir Processing. *Transactions of Nonferrous Metals Society of China (English Edition)* **2017**, *27* (4), 804–811. https://doi.org/10.1016/S1003-6326(17)60092-X.

(57) Akyuz, B. Influence of Al Content on Machinability of AZ Series Mg Alloys. *Transactions of Nonferrous Metals Society of China (English Edition)* **2013**, *23* (8), 2243–2249. https://doi.org/10.1016/S1003-6326(13)62724-7.

(58) Dinesh, S.; Senthilkumar, V.; Asokan, P.; Arulkirubakaran, D. Effect of Cryogenic Cooling on Machinability and Surface Quality of Bio-Degradable ZK60 Mg Alloy. *Mater Des* **2015**, *87*, 1030–1036. https://doi.org/10.1016/j.matdes.2015.08.099.

(59) Shi, K.; Ren, J.; Zhang, D.; Zhai, Z.; Huang, X. Tool Wear Behaviors and Its Effect on Machinability in Dry High-Speed Milling of Magnesium Alloy. *International Journal of Advanced Manufacturing Technology* **2017**, *90* (9–12), 3265–3273. https://doi.org/10.1007/s00170-016-9645-6.

(60) Chou, Y. K.; Liu, J. CVD Diamond Tool Performance in Metal Matrix Composite Machining. *Surf Coat Technol* **2005**, *200* (5–6), 1872–1878. https://doi.org/10.1016/j.surfcoat.2005.08.094.

(61) Devaraj, S.; Malkapuram, R.; Singaravel, B. Performance Analysis of Micro Textured Cutting Insert Design Parameters on Machining of Al-MMC in Turning Process. *International Journal of Lightweight Materials and Manufacture* **2021**, *4* (2), 210–217. https://doi.org/10.1016/j.ijlmm.2020.11.003.

(62) Venkatesh, R.; Hariharan, A.; Muthukrishnan, M. Machinability Studies of Al/SiC/ (20p) MMC by Using PCD Insert (1300 Grade). In *Proceedings of the World Congress on Engineering*; **2009**; Vol. 2, pp 1–4.

(63) Bachchhav, B.; Naranje, V. Effect of High Volume Fraction Reinforcement on Electro-Discharge Machining of Al-Al2O3MMC. *Mater Today Proc* **2021**, *43*, 753–759. https://doi.org/10.1016/j.matpr.2020.06.004.

(64) Manna, A.; Bhattacharyya, B. Investigation for Optimal Parametric Combination for Achieving Better Surface Finish during Turning of Al/SiC-MMC. *International Journal of Advanced Manufacturing Technology* **2004**, *23* (9–10), 658–665. https://doi.org/10.1007/s00170-003-1624-z.

(65) Balasubramanian, I.; Maheswaran, R.; Manikandan, V.; Patil, N.; Raja, M. A.; Singari, R. M. Mechanical Characterization and Machining of Squeeze Cast AZ91D/SiC Magnesium Based Metal Matrix Composites. In *Procedia Manufacturing*; Elsevier B.V., **2018**; Vol. 20, pp 97–105. https://doi.org/10.1016/j.promfg.2018.02.014.

(66) Pedersen, W.; Ramulu, M. Facing SiCp/Mg Metal Matrix Composites with Carbide Tools. *J Mater Process Technol* **2006**, *172* (3), 417–423. https://doi.org/10.1016/j.jmatprotec.2005.07.016.

(67) Kandemir, S.; Gavras, S.; Dieringa, H. High Temperature Tensile, Compression and Creep Behavior of Recycled Short Carbon Fibre Reinforced AZ91 Magnesium Alloy Fabricated by a High Shearing Dispersion Technique. *Journal of Magnesium and Alloys* **2021**, *9* (5), 1753–1767. https://doi.org/10.1016/j.jma.2021.03.029.

(68) Yang, X.; Huang, Y.; Barekar, N. S.; Das, S.; Stone, I. C.; Fan, Z. High Shear Dispersion Technology Prior to Twin Roll Casting for High Performance Magnesium/SiCp Metal Matrix Composite Strip Fabrication. *Compos Part A Appl Sci Manuf* **2016**, *90*, 349–358. https://doi.org/10.1016/j.compositesa.2016.07.025.

(69) Tzamtzis, S.; Zhang, H.; Hari Babu, N.; Fan, Z. Microstructural Refinement of AZ91D Die-Cast Alloy by Intensive Shearing. *Materials Science and Engineering A* **2010**, *527* (12), 2929–2934. https://doi.org/10.1016/j.msea.2010.01.013.

(70) Balvin, D.; Cressie, N.; Fitzmaurice, G.; Goldstein, H.; Johnstone, I. *Design and Analysis of Experiments*; Hinkelmann, K., Ed.; **2012**; Vol. 3. https://doi.org/10.1002/9781118147634.

(71) Box, G. E. P.; Draper, N. R. A Basis for the Selection of a Response Surface Design. *J Am Stat Assoc* **2012**, *54* (287), 622–654. https://doi.org/10.1080/01621459.1959.10501525.

(72) Ranade, S. S.; Thiagarajan, P. Selection of a Design for Response Surface. In *IOP Conference Series: Materials Science and Engineering*; **2017**; Vol. 263. https://doi.org/10.1088/1757-899X/263/2/022043.

(73) Kumar, V.; Kharub, M.; Sinha, A. Modeling and Optimization of Turning Parameters during Machining of AA6061 Composite Using RSM Box-Behnken Design. *IOP Conf Ser Mater Sci Eng* **2021**, *1057*, 1–11. https://doi.org/10.1088/1757-899x/1057/1/012058.

(74) Jaleh, B.; Fakhri, P. Infrared and Fourier Transform Infrared Spectroscopy for Nanofillers and Their Nanocomposites. *Spectroscopy of Polymer Nanocomposites* **2016**, 112–129. https://doi.org/10.1016/B978-0-323-40183-8.00005-7.

(75) Lakens, D.; Caldwell, A. R. Simulation-Based Power Analysis for Factorial Analysis of Variance Designs. *Adv Methods Pract Psychol Sci* **2021**, *4* (1), 1–14. https://doi.org/10.1177/2515245920951503.

(76) Kennedy Shaffer, L. Before $p < 0.05$ to Beyond $p < 0.05$: Using History to Contextualize p-Values and Significance Testing. *American Statistician* **2019**, *73*, 82–90. https://doi.org/10.1080/00031305.2018.1537891.

(77) Faraway, J. J. *Practical Regression and Anova Using R*; **2002**; Vol. 3.

(78) Kulaylat, A. N.; Tran, L.; Kulaylat, A. S.; Hollenbeak, C. S. *Regression Analysis*; **2023**. https://doi.org/10.1016/B978-0-323-90300-4.00087-2.

(79) Miles, J. R Squared, Adjusted R Squared. In *Wiley StatsRef: Statistics Reference Online*; **2014**. https://doi.org/10.1002/9781118445112.stat06627.

(80) Liu, D.; Liu, Z.; Zhao, J.; Song, Q.; Ren, X.; Ma, H. Tool Wear Monitoring through Online Measured Cutting Force and Cutting Temperature during Face Milling Inconel 718. *International Journal of Advanced Manufacturing Technology* **2022**, *122*, 729–740. https://doi.org/10.1007/s00170-022-09950-2.

(81) Macdonald, D. A. The Application of Focus Variation Microscopy for Lithic Use-Wear Quantification. *J Archaeol Sci* **2014**, *48*, 26–33. https://doi.org/10.1016/j.jas.2013.10.003.

(82) *HT2 series compression load cell*. Puls electronic. https://www.puls.com.tr/en/product/ht-2-series-low-profile-loadcell (accessed 2023-05-15).

(83) *IQ845 SYHU-07 : Square inserts with 8 cutting edges.* ISCAR. https://www.iscar.com/eCatalog/Item.aspx?cat=5667874&fnum=3327&mapp=ML&GFSTYP=I&srch=1 (accessed 2023-05-21).

(84) *IQ845 FSY-R07 50° face mills carrying screw clamped square Inserts with 8 cutting edges.* ISCAR. https://www.iscar.com/eCatalog/item.aspx?cat=3106523&fnum=3325&mapp=ML&app=60&GFSTYP=M&isoD=1 (accessed 2023-05-18).

(85) *MarSurf GD 140 Art. no. 6269010*. Mahr. https://metrology.mahr.com/en-us/products/article/6269010-rauheitsmessplatz-marsurf-gd-140/ (accessed 2023-05-19).

(86) Jadhav, S. S.; Kakde, A. S.; Patil, N. G.; Sankpal, J. B. Effect of Cutting Parameters, Point Angle and Reinforcement Percentage on Surface Finish, in Drilling of AL6061/Al2O3p MMC. *Procedia Manuf* **2018**, *20*, 2–11. https://doi.org/10.1016/j.promfg.2018.02.001.

(87) Ozben, T.; Kilickap, E.; Cakir, O. Investigation of Mechanical and Machinability Properties of SiC Particle Reinforced Al-MMC. *J Mater Process Technol* **2008**, *198* (1–3), 220–225. https://doi.org/10.1016/J.JMATPROTEC.2007.06.082.

(88) Jiang, R.; Chen, X.; Ge, R.; Wang, W.; Song, G. Influence of TiB2 Particles on Machinability and Machining Parameter Optimization of TiB2/Al MMCs. *Chinese Journal of Aeronautics* **2018**, *31* (1), 187–196. https://doi.org/10.1016/J.CJA.2017.03.012.

(89) Jebarose Juliyana, S.; Udaya Prakash, J. Drilling Parameter Optimization of Metal Matrix Composites (LM5/ZrO2) Using Taguchi Technique. *Mater Today Proc* **2020**, *33*, 3046–3050. https://doi.org/10.1016/J.MATPR.2020.03.211.

(90) Sap, S.; Uzun, M.; Usca, U. A.; Pimenov, D. Y.; Giasin, K.; Wojciechowski, S. Investigation of Machinability of Ti–B-SiCp Reinforced Cu Hybrid Composites in Dry Turning. *Journal of Materials Research and Technology* **2022**, *18*, 1474–1487. https://doi.org/10.1016/j.jmrt.2022.03.049.

APPENDIX A

CUTTING FORCE GRAPHS

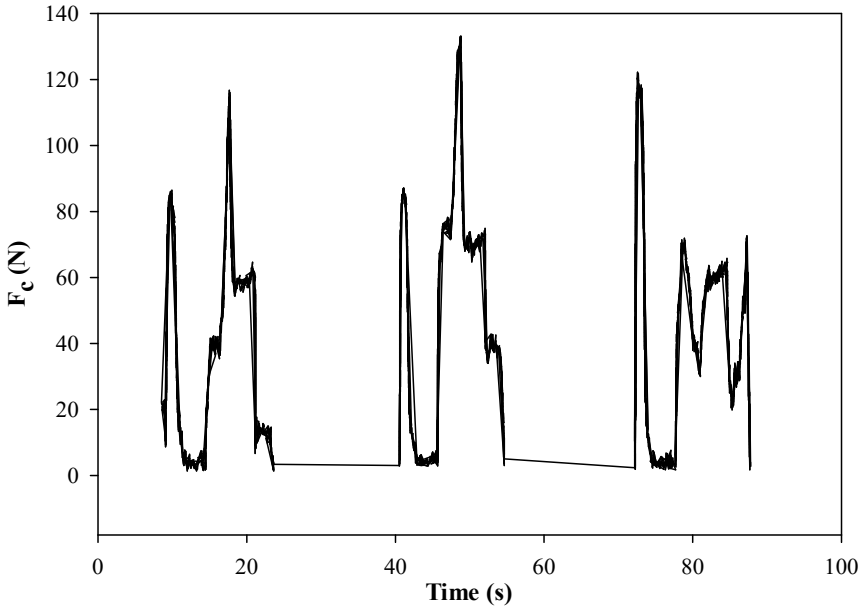

Figure 49. Cutting force graph of experiment 1

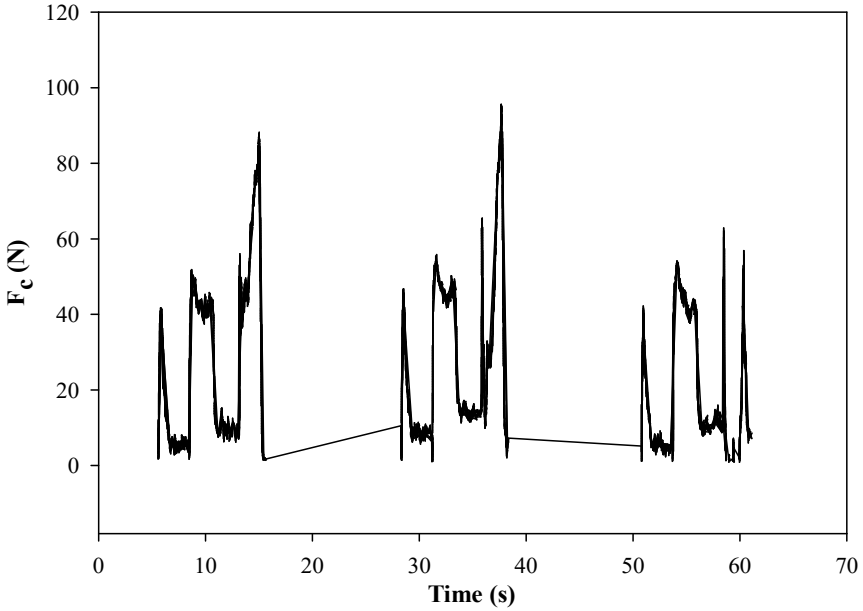

Figure 50. Cutting force graph of experiment 2

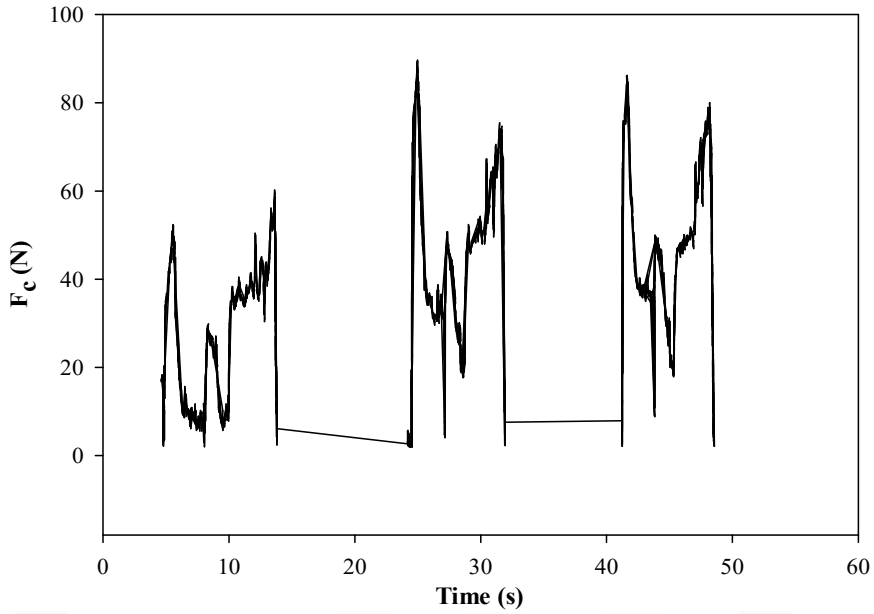

Figure 51. Cutting force graph of experiment 3

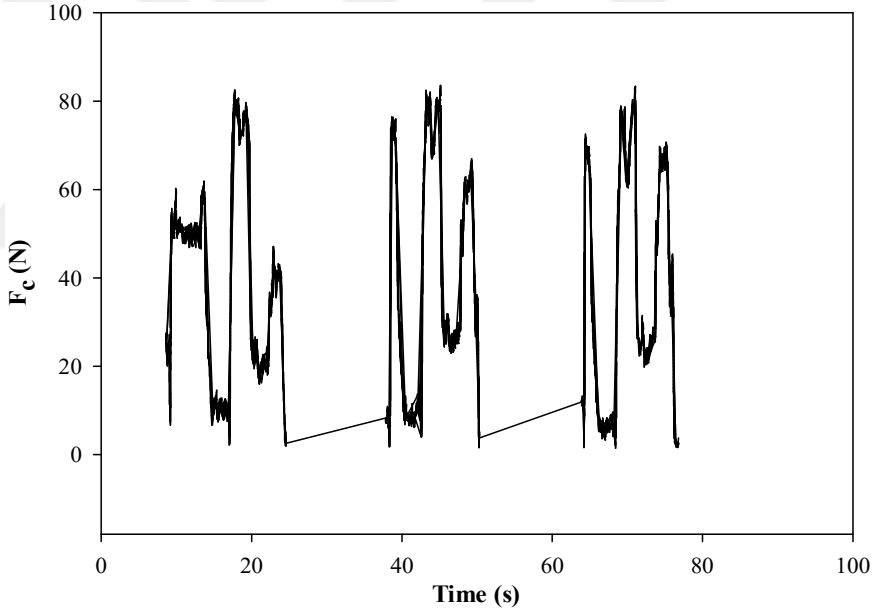

Figure 52. Cutting force graph of experiment 4

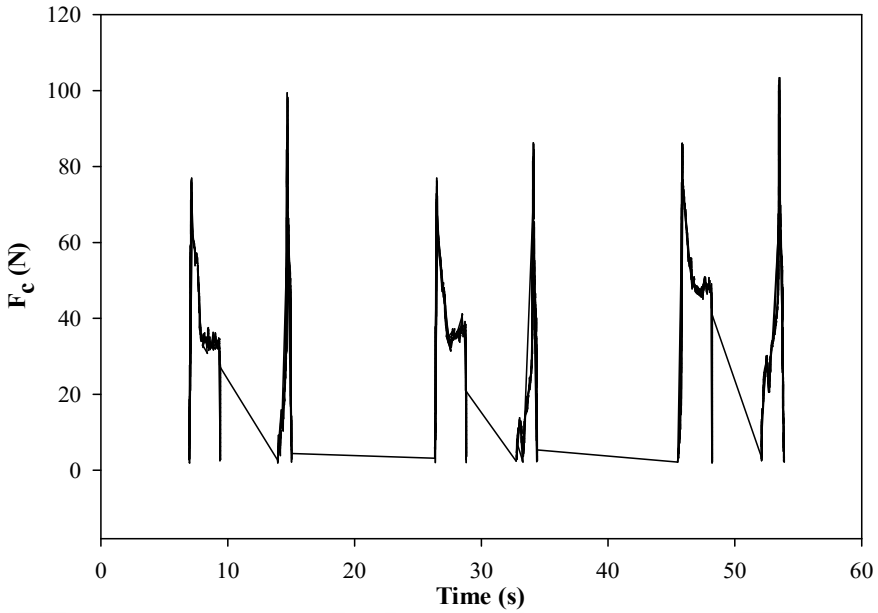

Figure 53. Cutting force graph of experiment 5

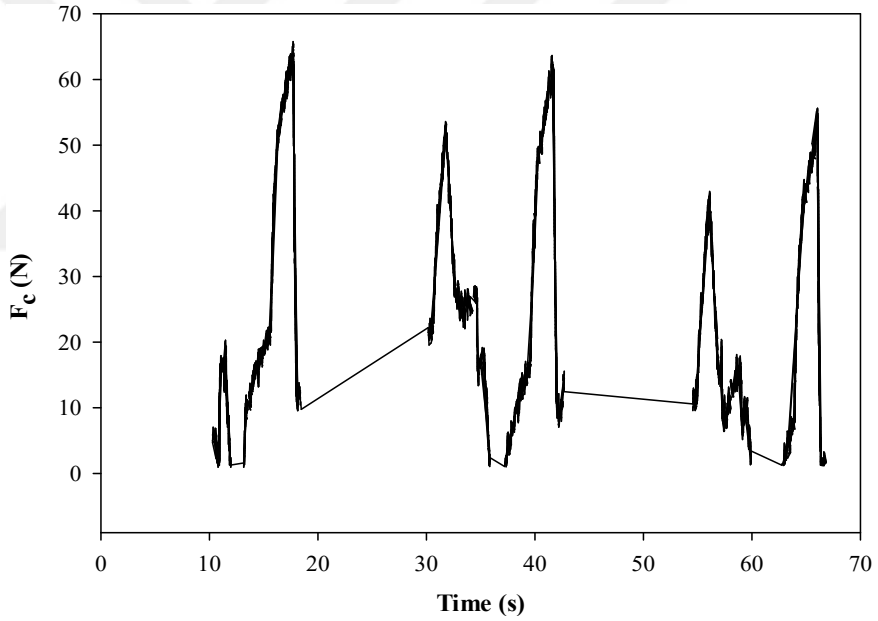

Figure 54. Cutting force graph of experiment 6

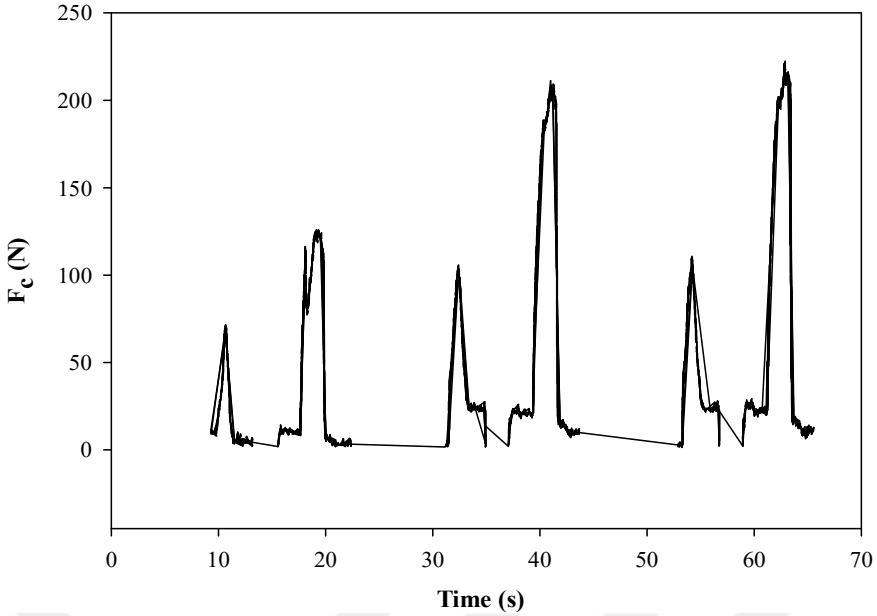

Figure 55. Cutting force graph of experiment 7

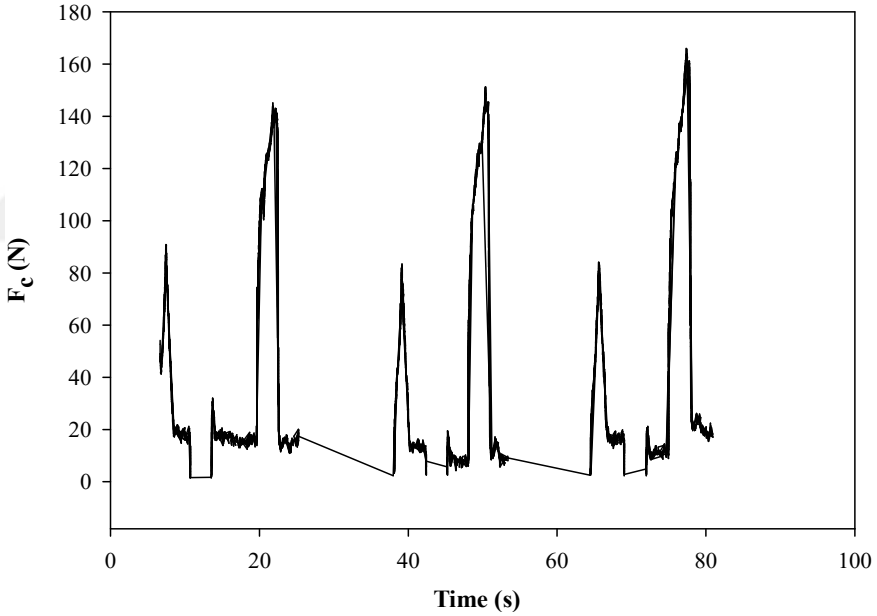

Figure 56. Cutting force graph of experiment 8

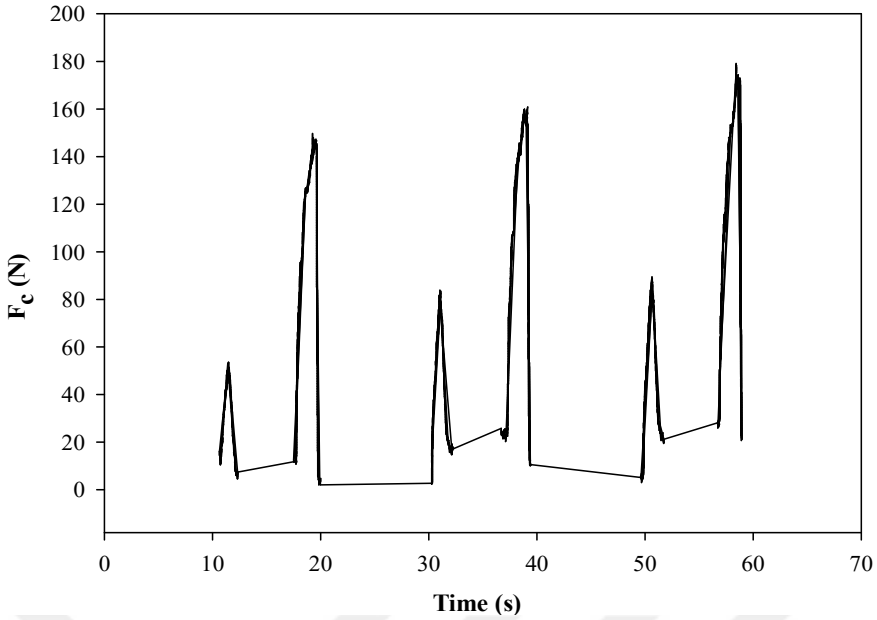

Figure 57. Cutting force graph of experiment 9